Bidispersity unlikely as a factor for the long runout of large mass flows: scale bias in analogue granular flow experiments

S. Makris[1,2,] †, I. Manzella[1,3,] ‡, and A. Sgarabotto[1,] §

[1] School of Geography, Earth and Environmental Science, University of Plymouth, Plymouth, UK.

[2] School of Geosciences, University of Edinburgh, Edinburgh, UK.

[3] Department of Applied Earth Sciences, Faculty of Geo-Information Science and Earth Observation (ITC), University of Twente, Enschede, The Netherlands.

Corresponding author: Symeon Makris (symeon.makris@plymouth.ac.uk)

†Current correspondence: makris.symeon@gmail.com, ORCID: 0000-0002-5718-8660

‡ ORCID: 0000-0001-7518-819X

§ ORCID: 0000-0002-4740-784X

Key Points:

- The potential for grain size distribution bimodality to contribute to the long runouts of granular flows is evaluated.
- Bimodality reduces the friction coefficient in experiments due to scale-dependent processes, not applicable to the scale of real events.
- Dynamic scaling of flow dynamics is important for the recreation of flow conditions in analogue experiments.

Abstract

The bidispersity observed in the grain-size distribution of rock avalanches and volcanic debris avalanches (rock/debris avalanches) has been proposed as a property contributing to their long runout. This has been supported by small-scale analogue experimental studies which propose that a small proportions of fine particles, mixed with coarser, enhances granular avalanche runout. However, the mechanisms enabling this phenomenon and their resemblance to rock/debris avalanches have not been directly evaluated. Here, binary mixture granular avalanche experiments are employed to evaluate the potential of bidispersity in enhancing runout. Structure-from-motion photogrammetry is used to assess centre of mass mobility. The findings suggest that the processes generating increased runout in small-scale avalanches are scale-dependent and not representative of rock/debris avalanche dynamics. In small-scale experiments, the granular mass is size-segregated with fine particles migrating to the base through kinetic sieving. At the base, they reduce frictional areas between coarse particles and the substrate, and encourage rolling. The reduced frictional energy dissipation increases kinetic energy conversion, and avalanche mobility. However, kinetic sieving does not occur in rock/debris avalanches due to a dissimilar granular flow regime. The proposition of this hypothesis overlooks that scale-dependent behaviours of natural events are omitted in small-scale experiments. At the small scale, a collisional regime enables the necessary agitation for kinetic sieving. However, rock/debris avalanches are unlikely to acquire a purely collisional regime, and rather propagate under a frictional regime, lacking widespread agitation. Therefore, bidispersity is unlikely to enhance the mobility of rock/debris avalanches by enabling more efficient shearing at their base.

Plain Language Summary

Large landslides like rock avalanches and volcanic debris avalanches flow unexpectedly long distances before stopping. The mechanisms generating this phenomenon remain unknown. The fact that they contain large proportions of finer and coarser particles (with relatively smaller quantities of the sizes between them) has been suggested by experiments to be a potential factor for the long distances they cover. In this work, we have carried out experiments to examine the processes enabling this event at the scale of lab experiments, in order to assess their potential in real events. We found that the phenomenon is caused by fine particles percolating to the base of the flow. There, they reduce the surface of the coarse particles which is in contact with the substrate, and also encourage the rolling of the coarser particles. This reduces frictional energy loss, and conserves more energy which contributes to the flow, leading to longer distances. However, the conditions which allow these processes and the percolation of the fine particles to the base are scale-dependent and are not applicable to large-scale events. When planning granular flow experiments or interpreting their findings the scaling is important to ensure similarity between the experimental conditions and the physical processes targeted.

1. INTRODUCTION

Rock avalanches are rapid mass movements that evolve from the detachment of a rock mass which disaggregates into a granular flow during propagation (Hungr et al., 2014; Scott et al., 2001). Volcanic debris avalanches are the equivalent mass flow in volcanic environments,

mobilising volcanic material, after the collapse of unstable volcanic flanks (Roverato et al., 2021; Ui, 1983). The two events (subsequently rock/debris avalanches collectively) share some characteristics. Both achieve much greater horizontal runout distance compared to their fall height (Davies, 1982; Hungr, 2002; Legros, 2002), far greater than predicted by simple frictional models of a coherent sliding mass (Rait and Bowman, 2016). To explain the long runout, a mechanism that accounts for the apparent decrease in the effective friction coefficient is required. Many theories have been proposed to explain this mechanism, but none are consistent with field observations (reviewed in Legros, 2002; Collins and Melosh, 2003; Friedmann et al., 2006; Manzella and Labiouse, 2008, 2009; Davies and McSaveney, 2012). The issue remains controversial and unresolved (Banton et al., 2009; Cabrera and Estrada, 2021; Davies and McSaveney, 2012; Perinotto et al., 2015; Pollet and Schneider, 2004), demanding an evaluation of theoretical models of granular avalanche propagation in comparison to real events.

Propagating rock/debris avalanches are believed to behave as dense granular flows where grain interactions are the most important energy dissipation process (Campbell, 1990; Davies and McSaveney, 1999; Makris et al., 2020; Reubi and Hernandez, 2000; Schneider and Fisher, 1998; Voight et al., 1983). Recent work supports that rock/debris avalanches behave as ideal granular avalanches where fluid effects are negligible (e.g. Legros, 2002; Makris et al., 2020). The flow is characterised by a distributed shear motion where individual particles interact with each other and the flow boundaries (Dufresne and Davies, 2009; Iverson, 1997; Pierson and Costa, 1987). Flow dynamics are controlled by particle interactions, internal and basal friction coefficients, and interactions with flow boundaries and path geometry (Denlinger and Iverson, 2001; Roche et al., 2021). The energy exchange, referred to as the granular effect, is driven by particle interactions, resulting in momentum transfer and dissipation (Hu et al., 2020). The magnitude of the energy exchange is measured as the granular temperature (Campbell, 1990; Iverson, 1997; Sanvitale and Bowman, 2016). The granular effect is a function of the particles' shape, density, size, hardness and roughness (Bartali et al., 2015) and the flow processes controlling their interactions. Therefore, grain-size distribution properties can potentially affect propagation dynamics.

Natural granular flows including rock/debris avalanches contain a wide range of particle sizes (Hungr et al., 2014; Phillips et al., 2006; Yang et al., 2015). Rock/debris avalanche deposits are composed of angular/subangular clasts spanning a size range from fine particles smaller than 1 μm up to tens of metres (e.g. Voight, 1978; McSaveney and Davies, 2002; Roche et al., 2006; Makris et al., 2023a). Even in cases where the source material is homogeneous in terms of particle size, heterogeneity can arise from fragmentation and comminution during propagation (Crosta et al., 2007; Davies and McSaveney, 2012; De Blasio and Crosta, 2014; Dufresne and Dunning, 2017; Knapp and Krautblatter, 2020; McSaveney and Davies, 2002). Furthermore, rock/debris avalanche deposits are characterised by bidisperse to polydisperse grain-size distributions (e.g. Scott et al., 1995; Glicken, 1996; Vallance, 2000; Pollet and Schneider, 2004; Vallance and Iverson, 2015; Bernard et al., 2017). Bidispersity implies the existence of two dominant particle sizes or size ranges. Bidispersity is exhibited in volcanic debris avalanche deposits, at least locally (Bernard and van Wyk de Vries, 2017; Glicken, 1996; Siebert, 2002; Siebert et al., 1989; Ui and Glicken, 1986); while in the case of rock avalanches, bidispersity develops especially in zones of concentrated shear stresses (Dufresne and Dunning, 2017). This is supported by analogue experiments suggesting that bidisperse distributions are generated with increased shear stresses or confining pressures (Caballero et al., 2014; Iverson et al., 1996). Recent studies have supported that a bidisperse grain-size distribution is capable of providing a more energy-efficient shear accommodation arrangement, reducing frictional losses at the base

of rock/debris avalanches. Studies including Linares-Guerrero et al. (2007), Yang et al. (2015), and more recently Bartali et al. (2020), Hu et al. (2021) and Duan et al. (2022) propose bidispersity as a contributing factor to the long runouts.

Laboratory experiments can provide important information on the propagation processes of granular avalanches despite idealised experimental conditions (Davies and McSaveney, 1999; Dufresne, 2012; Longchamp et al., 2016; Manzella and Labiouse, 2013, 2009, 2008; Shea and van Wyk de Vries, 2008). Column collapse and granular avalanche experiments (e.g. Phillips et al., 2006; Goujon et al., 2007; Moro et al., 2010; Degaetano et al., 2013; Yang et al., 2015; Hu et al., 2020; Li et al., 2021), as well as numerical models (e.g. Linares-Guerrero et al., 2007; Cabrera and Estrada, 2021; Hu et al., 2021), have been employed to study the behaviour of granular mixtures composed of more than one particle sizes. Analogue experiments such as those of Goujon et al. (2007), Yang et al. (2015), Bartali et al. (2020), Hu et al. (2020) and Duan et al. (2022) evaluate the behaviour of granular avalanches (i.e. not column collapse) composed of combinations of two size species of particles (binary and bidisperse) at various proportions. Such studies have observed that the addition of a small proportion of finer particles to a granular mixture generates enhanced runouts under particular conditions (e.g. Roche et al., 2006; Moro et al., 2010; Yang et al., 2015; Duan et al., 2022). Although empirical relationships between single parameters under bidispersity have been established, limited attention has been given to the particle interaction mechanisms affecting energy dissipation and mobility (Li et al., 2021). Even less consideration has been taken regarding the applicability of the relevant granular effects to natural, large-scale geophysical flows, which has not been directly addressed so far.

The current study evaluates the impact of bidisperse grain-size distributions on the propagation processes and energy dissipation in small-scale analogue granular flow experiments by combining different binary particle size mixtures. The combined effect with volume, inclination, and size ratio between particles is also evaluated. Moreover, the impact of a slope-break between the inclined plane and the horizontal emplacement surface is considered. The propagation of the centre of mass and frontal velocity are examined in order to evaluate the mechanisms responsible for the runout of granular avalanches. By examining the dynamics of the modelled avalanches this study constrains the processes under which bidispersity enhances mobility. Subsequently, the potential of these processes as a factor for the enhanced mobility of rock/debris avalanches and other natural geophysical flows is evaluated.

2. BIDISPERSITY AND MOBILITY - BACKGROUND

Lab-scale analogue experiments suggest that granular avalanches containing more than one particle size (i.e. bidisperse or polydisperse) diverge in their macroscale properties from avalanches with monodisperse grain-size distributions (e.g. Reubi et al., 2005; Phillips et al., 2006; Roche et al., 2006; Goujon et al., 2007; Yang et al., 2015). One of the main differences, commonly observed, is that the addition of a small fraction of fine particles to a mass composed of coarser results in increased velocity and runout of the centre of mass and the front of avalanches (e.g. Phillips et al., 2006; Roche et al., 2006; Degaetano et al., 2013; Yang et al., 2015). The proportion of fine particles to the total mass is denoted as ψ. Analogue experiments suggest that maximum frontal runout is achieved at a critical ψ value (ψ_{CRf}) (e.g. Phillips et al., 2006; Moro et al., 2010; Kokelaar et al., 2014; Bartali et al., 2020; Hu et al., 2020). The ψ_{CRf} has been suggested under the bidisperse experimental conditions of Phillips et al. (2006), Roche et

al. (2006), and Hu et al. (2020) to be equal to 0.30. In the experiments of Moro et al. (2010), ψ_{CRf} was equal to 0.25; for Degaetano et al. (2013) 0.50, and Duan et al. (2022) 0.05. The ψ_{CRf} was found to be variable according to the granular size composition and other experimental conditions, such as slope inclination of the flow path by other studies (Goujon et al., 2007; Yang et al., 2015). A comparison of the experimental conditions of these studies is presented in Appendix I. It should be noted that the value of ψ_{CRf} enabling maximum frontal runout is not always equal to the ψ value which enables maximum displacement of the centre of mass (ψ_{CRCoM}).

The investigation of the mechanisms facilitating the increased runout effect by Phillips et al. (2006) reveals that in small-scale avalanches fine particles migrate rapidly to the base. Once at the base, fine particles reduce the frictional areas between the coarse particles and the substrate by occupying the area between them and acting as 'ball-bearings' (Linares-Guerrero et al., 2007; Roche et al., 2006). They simultaneously act as 'rollers' to encourage rolling as opposed to frictional sliding (Hu et al., 2021; Phillips et al., 2006). Rolling reduces the friction coefficient at the base of the flow as it is less expensive in terms of energy dissipation, and increases the efficiency of kinetic energy transfer (Hu et al., 2021, 2020; Phillips et al., 2006). This process finds support in numerical modelling of binary size distributions granular avalanches where rotational motion is enhanced at their base (Hu et al., 2021; Linares-Guerrero et al., 2007). In effect, a basal layer of fine particles reduces the friction coefficient between the granular body and the propagation surface (Lai et al., 2017), inhibiting frictional energy losses.

However, this idealised behaviour has to be linked to the scale and processes of natural events. One hypothesis connecting bidispersity and the mobility of rock/debris avalanches has been supported by the studies of Linares-Guerrero et al. (2007), Yang et al. (2015), Lai et al. (2017), Hu et al. (2021) and Duan et al. (2022) and suggests that fine particles migrate and lubricate the base, in a process identical to the described lab experiments. Fine particles enable rolling instead of sliding, locally accommodating shear stress with the rest of the mass carried, sliding on the basal layer, without experiencing agitation or shear stress (Hu et al., 2021). An alternative hypothesis involves the sedimentology of shear zones observed in the field. Bidispersity is observed in rock/debris avalanches, especially in shear zones of magnified shear stresses (Dufresne and Dunning, 2017; Glicken, 1996). The concentrated accommodation of shear, principally in shear zones with the efficient bidisperse arrangement, can potentially be a contributing mechanism for long runouts. Shear zones are found primarily in the basal domains, but also within the body of rock/debris avalanches (Dufresne and Dunning, 2017; Hewitt, 2002; Roverato et al., 2015; van Wyk De Vries et al., 2001; Weidinger et al., 2014). They are suggested to focus shear and act as corridors of shear accommodation (Crosta et al., 2007; Paguican et al., 2021; Roverato et al., 2015). Areas protected from shear maintain a quasistatic behaviour with low energy dissipation. Li et al. (2021 - pp 1793) propose that the bidisperse arrangement of shear zones potentially efficiently accommodates shear limiting frictional losses. This shear concentration limits overall frictional losses in the system. However, further evaluation of both suggested hypotheses is required to understand their potential and the mechanisms by which bidispersity could enhance mobility in natural granular flows.

201

202 ## 3. METHODOLOGY

203 ### 3.1 Experimental setup and measuring systems

204 The setup is comprised of a 1.5 m long inclined plane and a 2.0 m horizontal depositional surface
205 (fig. 1a). The material is laterally confined throughout the propagation by transparent plastic
206 walls, limiting its width to 0.3 m. The smoothness of the walls and the fact that the ratio between
207 the mean particle diameter (of even the largest size species) and the flow width is <1/20 ensure
208 that there is no boundary effects (Ahmadipur et al., 2019; Jiang and Zhao, 2015; Schilirò et al.,
209 2019; Valentino et al., 2008). Even though confined avalanches do not exhibit the flow and
210 depositional morphologies of unconfined, the purpose was the detailed examination of the effect
211 of individual processes and not the recreation of deposit geometry. The confinement did not
212 permit lateral spreading, however, it is assumed that there is no significant effect on the flow
213 dynamics in the flow direction (Thompson et al., 2009 - pp246). The inclination of the inclined

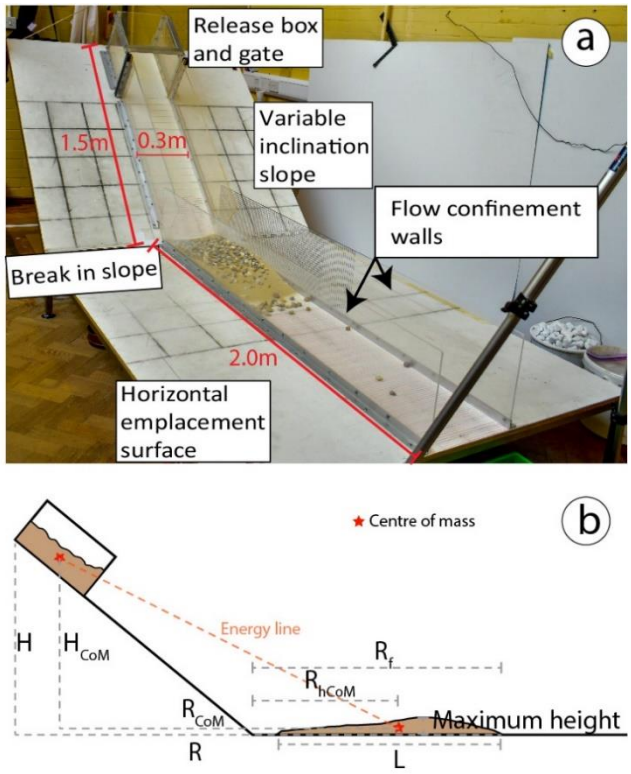

Figure 1 ***a*** *Experimental setup.* ***b*** *Measurements and descriptors of the deposit and propagation. H: fall height from the highest point of the material in the box to the horizontal plane; H_{CoM}: fall height of the centre of mass (CoM). R: avalanche front runout from the release position; R_{CoM}: centre of mass runout from the release position. R_f: avalanche front runout on the horizontal plane; R_{hCoM}: centre of mass runout on the horizontal plane. The energy line links the position of the centre of mass before release and in the final deposit (adapted from Manzella and Labiouse, 2009).*

plane was varied between 35°, 40° and 45°. The geometry of the slope-break between the incline and horizontal surfaces is dictated by this inclination.

Prior to release, the material was held in a release box with a sluice gate removable by sliding upwards. The rapid removal of the gate initiates the flow of material on the inclined plane. After propagating down the incline, the material interacts with the slope-break and subsequently propagates on the horizontal surface. The final deposit is formed when all material is immobilised. Propagation is defined as the flow of the material after the release in the incline and horizontal planes. The final deceleration and deposition of the material is defined as the emplacement stage.

Measurements of the geometry of the material prior to release were made manually and photographs were taken so that the location of the pre-release centre of mass could be calculated. Manual measurements were taken for the frontal runout (R_f), the length of the deposit (L) and the maximum height of the final deposit (fig. 1b). R_f is defined as the distance travelled by the most distal position on the horizontal plane from the slope-break, where particles are still in contact with the main deposit body. However, for confirmation and higher accuracy measurements, an oblique photogrammetry survey was conducted, as in Li et al. (2021). Photographs of the final deposit were processed in the commercially available software *Agisoft Metashape* generating a 3D model. A digital elevation model (Appendix II) allowed calculating the average deposit thickness, the location of the centre of mass of the deposit, the length of the deposit L, and R_f.

Two high-definition cameras recorded the avalanches, one frontal and one lateral (as illustrated in Appendix III). The lateral camera view (25 fps, HDV 1440 x 1080) was used to observe the interaction of the avalanche with the slope-break. The frontal velocity (Vf) was obtained through the analysis of 50 fps (FHD 1920 x 1088) footage. The location of the front of the flow at each frame was manually located, and the displacement between frame intervals calculated. A moving average is used in the presented time series, with a period of three frames to smooth out short-term fluctuations and highlight longer-lasting trends. Only one of the runs is illustrated in figures 4 and 6, for clarity of illustration. The repeatability of the experiments was ensured by confirming each of the minimum of three runs.

H/R (often H/L in the literature) is the ratio between the fall height from the highest point of the material in the box to the horizontal plane (H) and the horizontal runout of the front of the avalanche from the front of the material pre-release (R – see fig. 1). This ratio is used as a measure of avalanche mobility in landslide literature (initially by Heim, 1932). Although it is often calculated as the distance between the furthest location of the scarp and the toe of the deposit, in this study it is also calculated for the height fallen (H_{CoM}) and horizontal displacement (R_{CoM}) by the centre of mass, as H_{CoM}/R_{CoM} (also referred to as the gradient of the energy line) (Legros, 2002). H_{CoM}/R_{CoM} is not usually used in field studies because it is difficult to determine in natural deposits (Bowman et al., 2012). However, the displacement of the centre of mass is a better measure when considering energy dissipation, as it excludes the effect of spreading of the

mass on R (Davies, 1982). Following studies such as Goujon et al. (2007), Yang et al. (2015) and Hu et al. (2020) the proportion of material was assigned by weight (rather than volume). Therefore, also due to the differences in mass configuration (i.e., pore spaces between the coarse particles are sometimes void and sometimes filled by the finer particles), the volume of the material was not identical in all experiments, as illustrated in fig. 2. Normalised runout (R_n) is used to illustrate and compare findings. The R_n is represented by the equations $R_n=R_f/h^*$ and the

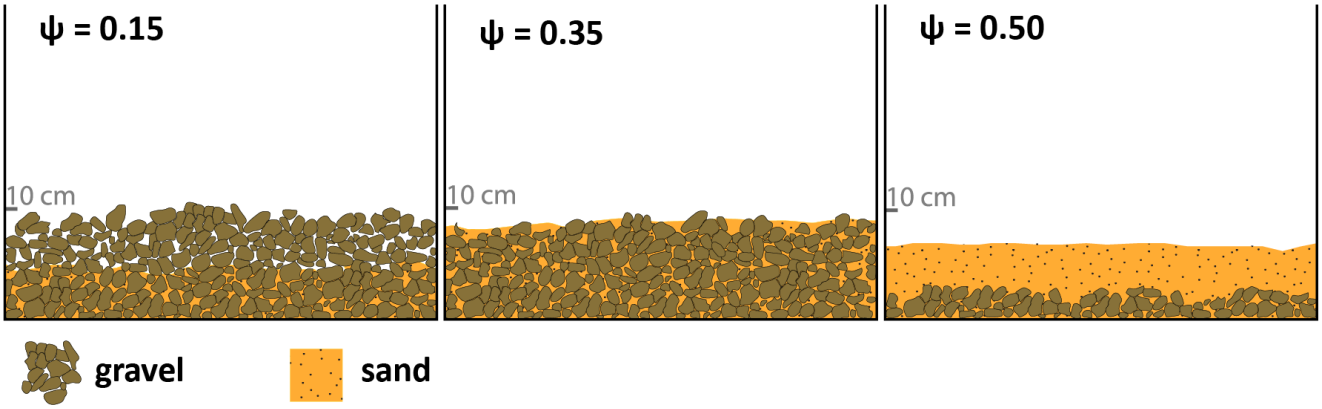

Figure 2 Schematic representation of the pre-release arrangement of material in the release box. Note the difference in volume at different size combinations (although weight is equal), as well as the pore spaces between coarse particles at low fractions of fine particles (ψ).

normalised propagation of the centre of mass by $R_{nCoM}=RC_{oM}/h^*$, where the R_f and the R_{CoM} are normalised by the cubic root of the volume of the material ($h^* = V^{1/3}$). Davies and McSaveney (1999) suggest that such normalised quantities can be compared to real events. Total spreading (S_n) is measured as the normalised L of the final deposit, $S_n=L/h^*$ (Manzella and Labiouse, 2013). The normalised distance between R_f and the propagation of the centre of mass on the horizontal plane (R_{hCoM}) was also used here ($S_f=(R_f-R_{hCoM})/ h^*$) as a measure of the spreading at the front of the deposit (S_f) which is not affected by material left behind or piled on the slope during the emplacement stage.

3.2 Scaling

Scaling is critical in designing experiments and correlating the findings of small-scale granular avalanches to natural geophysical mass flows (Iverson, 2015; Iverson et al., 2004). The similarity between analogue models and real events must be addressed by introducing geometric and dynamic dimensionless parameters to satisfy the continuum hypothesis (Iverson, 2015, 1997; Manzella and Labiouse, 2013; Shea and van Wyk de Vries, 2008). Geometric parameters refer to the size and morphology of the particles and the avalanche system. Dynamic parameters refer to the ratio between forces within the avalanche, which are later discussed. The presented experiments follow the scaling considerations of the mentioned previous studies.

Firstly, particle size is large enough to reduce the impact of electrostatic effects to negligible levels (Davies and McSaveney, 1999; Drake, 1991; Iverson and Denlinger, 2001; Manzella and

Labiouse, 2009). Additionally, it is assumed there is a similarity to large-scale avalanches regarding the geometric shape, air and grain densities and drag coefficient between grains and air (Davies and McSaveney, 1999). Moreover, Drake (1991) suggests that the avalanche depth needs to be at least ten times larger than the mean particle diameter, which is also fulfilled. If these conditions are met, it is believed that the findings can contribute to the understanding of natural geophysical granular avalanches (Manzella and Labiouse, 2013). These are the scaling guidelines most consistently followed by granular avalanche experiments and the present study. Geometric and dynamic scaling effects are further addressed in the discussion.

3.3 Material and experimental conditions

The material used in this study consists of four different granular sizes composed of subrounded gravels and subangular corundum sand (Appendix IV). Angular-subangular natural rock material has been used in an attempt to maintain a close approximation to the modelled phenomena (Cagnoli and Romano, 2010; Davies and McSaveney, 1999; Li et al., 2021; Shea and van Wyk de Vries, 2008). The properties of the material used are reported in the supplementary Appendix IV.

For the bidisperse experiments, a proportion (by mass) of finer granular material was added to the mass composed of coarser particles. For each set of experiments, this proportion ψ of fine material mass was varied between $\psi=0$ (all coarse) and $\psi=1$ (all fine). Prior to the initiation of the avalanche, coarse and finer particles were placed in the release box so that the fine particles filled the pore spaces between the largest particles from the bottom up (fig. 2). In cases where low quantities of fine material were used, void pore spaces remained at the top of the material (fig. 2). Conversely, when the volume of the fines was greater than the pore space between the coarse, excess fines were positioned above the coarse material.

For each ratio of fine material, other factors were changed in order to additionally examine the effect of bidispersity combined with different parameters. These were volume, inclination and different grain sizes. The experiments are divided into five series according to the parameters under examination. All the experimental conditions are illustrated in table 1. Each experiment was repeated a minimum of three times to generate data to be averaged and to ensure their reproducibility.

Experiment series	GRAVEL 9.5-16mm	GRAVEL 16-22.4mm	SAND 0.355-0.50mm	SAND 0.5-1mm	Mass (kg)	Inclination (°)
A		-	-		20	40
B		-	-		40	40
C		-	-		20	35
D		-	-		20	45
E	-			-	20	40

Table 1 The five experimental series examining different parameters.

4. RESULTS

4.1 Morphology

Under all the conditions of bidisperse granular avalanches, the following common morphological features are observed. At low ψ values (ψ<0.5-0.15 depending on experimental conditions) the addition of fines causes the final deposits to initially become longer (normalised length=L/h*) and lower in height (normalised average height=average height/h*) compared to avalanches composed solely of coarse particles (e.g. fig. 3). They also achieve greater runouts (fig. 3: 0.00 – 0.15). At a critical value of ψ_{CRf}, maximum R_f is achieved (fig. 3: 0.15). However, further increase of ψ, progressively results in a decreased R_f (fig. 3> 0.15). With progressively higher ψ (ψ>~0.8) a stage is reached where L is smaller and deposit thickness is higher than the monodisperse flow composed entirely of coarse particles. At low ψ values, coarse particles travel

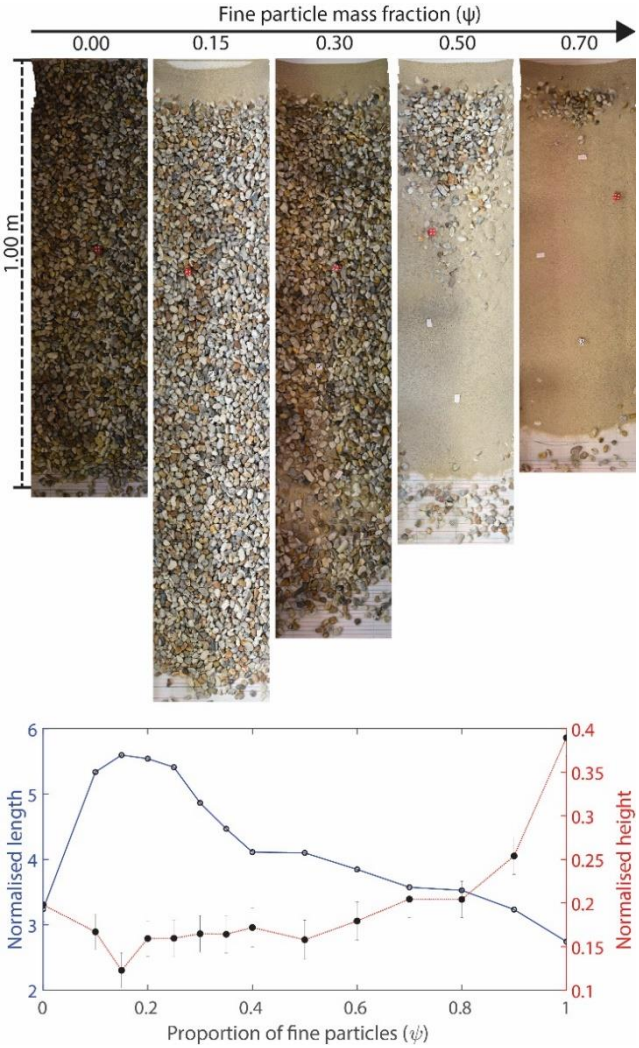

Figure 3 ***TOP****: Orthophotos of the deposits of experimental avalanches in series A illustrating their runout and morphology. The flow direction is downwards.* ***BOTTOM****: Normalised length and height of the experimental avalanches of series A.*

with the fine forming a continuous cover over the deposit surface (fig. 3: 0.00 – 0.30). At higher

ψ they are emplaced at the rear of the deposit near the slope-break (fig. 3: 0.50-0.70). An exception arises when coarse particles that separate from the avalanche early and travel independently, deposited in front of it.

4.2 Frontal velocities

According to Rait and Bowman (2016), in rock avalanches, the main phases are: the acceleration under gravity phase, and the phase of deceleration of the avalanche after its impact with the near-horizontal valley floor. For the purposes of the analysis of propagation dynamics and energy dissipation, these phases are here considered separately, and the second phase is further subdivided to address the effect of the slope-break. The Vf is therefore divided temporally into three parts from the release of the material through propagation and up to their emplacement. These phases are exhibited, with variation according to the experimental conditions, in all the experiments (fig. 4):

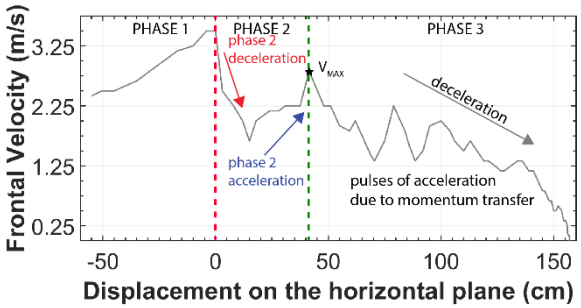

Figure 4 The frontal velocity of the fine particle content of ψ=0.15 avalanche of experimental series B with the velocity phases annotated. V_0: frontal velocity at the slope-break; V_{MIN}: lowest frontal velocity of phase 2; V_{MAX}: velocity the front accelerates to at the end of phase 2.

PHASE 1 – ACCELERATION ON THE INCLINED SLOPE: This is the stage of acceleration following the release of the material. This phase ends when the material at the front of the avalanche interacts with the slope-break to begin their transition to the horizontal plane.

PHASE 2 – INTERACTION WITH THE SLOPE-BREAK: This phase begins when the avalanche front first interacts with the geometric irregularity of the slope-break and suffers a deceleration. This deceleration is followed by a rapid acceleration as the material behind the front (greater in mass) transfers momentum to the front. This can be observed the video frames of the avalanches illustrated in fig. 5. Once the acceleration reaches peak velocity (V_{MAX}) in phase 2, and starts decelerating again, phase 2 ends. This is when the material at the front stops receiving energy directly from the momentum of material interacting with the slope-break. The peak velocity V_{MAX} in phase 2 is not reached again by the flow.

Phase 2 deceleration is calculated here as the rate of velocity change between the interaction of the front with the slope-break (V_0) and the recording of the minimum velocity of phase 2 (V_{MIN}), as in the equation:

$$\text{Phase 2 percentage deceleration} = \frac{V_0 - V_{MIN}}{V_{MIN}} \quad (Eq.\ 1)$$

where V_0 is the frontal velocity at the slope-break, and V_{MIN} is the lowest frontal velocity of phase 2 (fig. 4). Phase 2 acceleration is calculated as the rate of velocity change between the lowest velocity of phase 2 and the velocity the front accelerates to at the end of phase 2 (V_{MAX}):

$$\text{Phase 2 percentage acceleration} = \frac{V_{MAX} - V_{MIN}}{V_{MIN}} \quad (Eq.\ 2)$$

where V_{MAX} is the velocity the front accelerates to at the end of phase 2 (fig. 4).

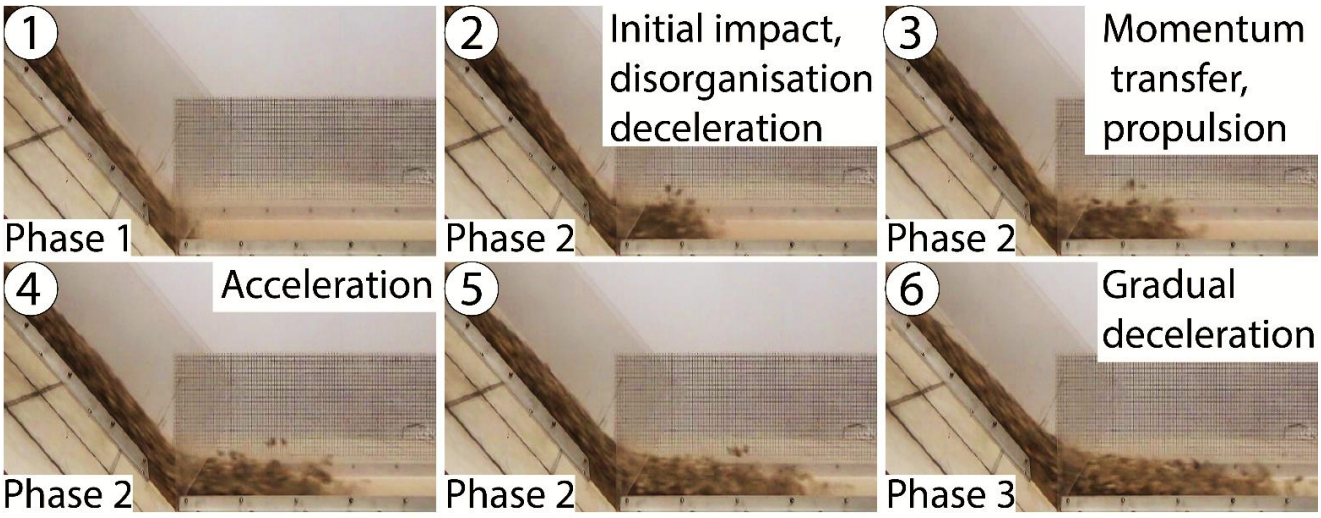

Figure 5 Frames from the interaction of the front of the avalanche (ψ=0.15, series B) with the slope-break.

PHASE 3 – DECELERATION AND EMPLACEMENT: After the interaction with the slope-break stops disturbing the front of the flow, a deceleration phase eventually leads to the emplacement of the material. This phase is characterised by pulses of deceleration of the frontal material and subsequent acceleration (fig. 4). The Vf is lower for each subsequent pulse. The amplitude of these waves appears to be a function of the volume of the granular mass, as later discussed. Phase 3 ends when the material comes to a halt after losing momentum and energy and each particle settles in its position in the final deposit. Phase 3 deceleration is calculated here as the average rate of velocity change between the initiation of phase 3 and the final deposition (fig. 4):

368 $$\text{Phase 3 average deceleration} = \frac{V_{MAX}}{time\ duration\ of\ phase\ 3}$$

369 *(Eq. 3)*

370

4.3 Fine particle content (ψ)

Experiment series A (table 1) has the primary aim of examining the impact of ψ on the runout and the mobility of the centre of mass. It is also the reference case for the rest of the experiments. Fig. 6a illustrates that changes in ψ result in variation of both the R_n and R_{nCoM} propagation metrics. The initial addition of fines for ψ=0.10 leads to an increase of R_n and R_{nCoM}. The maximum R_n exhibited at ψ_{CRf}=0.15 represents an increase of 87% from the all-coarse avalanche. In the case of the centre of mass, at ψ_{CRcom}=0.10 the equivalent increase is ~100%. There is, therefore, a divergence in ψ value for the maximum R_n in comparison to the maximum R_{nCoM}. Further increases in ψ, past ψ_{CRf} and ψ_{CRcom}, result in reduced R_n and R_{nCoM} (fig. 6a). Greatest R_n and R_{nCoM} variability is observed at ψ between 0.10 and 0.35. However, R_n and R_{nCoM} remain above the all-coarse avalanche up to ψ=0.80. The sensitivity of R_n and R_{nCoM} to ψ decreases after all the pore spaces between the coarse particles are filled by fines at ψ=0.35 (fig. 6a). These observations are confirmed by fig. 6b. The H/R and H_{CoM}/R_{CoM} measure propagation including the location of the mass before their release and confirm that the relationships are not an effect of the initial position of the centre of mass. Fig. 6c illustrates that spreading S_n and S_f are greater at ψ=0.15. The value of ψ appears to greatly affect the degree of spreading when there are pore spaces between the coarse particles (ψ<0.35). Once the pore spaces are completely filled

388 up with fine particles, ψ variation has less impact on spreading (fig. 6c). Particularly the S_f
389 remains almost constant after pore spaces are filled.

390 Vf observations suggest that ψ affects phase 2 (interaction with the slope-break) and phase 3
391 (deceleration and emplacement). There does not appear to be a systematic impact on phase 1
392 (acceleration on inclined slope, fig. 6d). In phase 2, the deceleration after the slope-break is
393 consistently increased with increasing ψ (fig. 6e). Phase 2 acceleration increases with ψ between
394 0.10 and 0.35. In this range increases in ψ result in lower acceleration (fig. 6e). The average

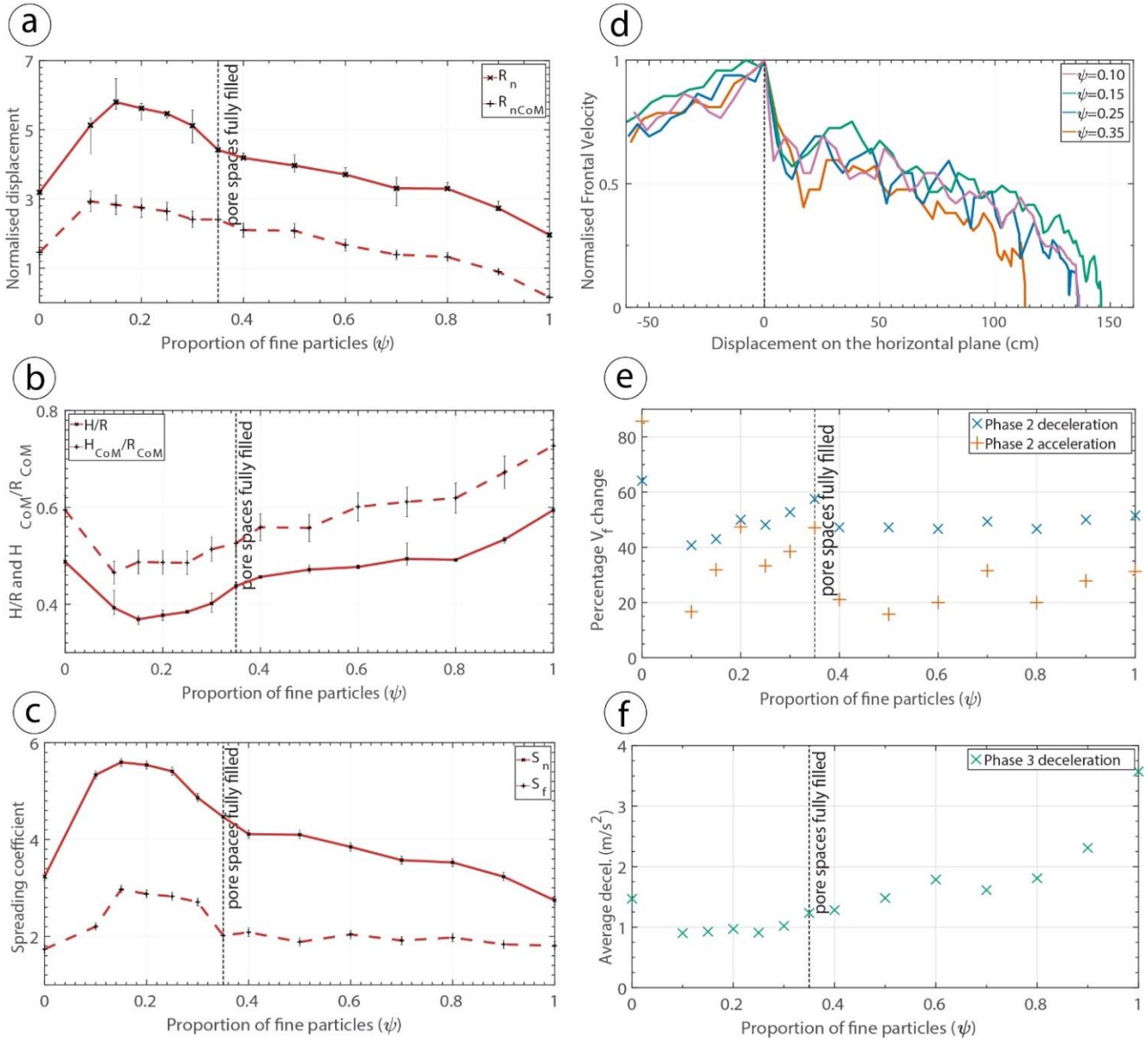

Figure 6 ***(a-c)*** *Results from experimental series A.* ***a*** *Frontal runout (R_n) and propagation of the centre of mass (R_n) at different proportions of fines (ψ).* ***b*** *H/R and H_{CoM}/R_{CoM} at different proportions of fines ψ.* ***c*** *Total spreading (S_n) and frontal spreading (S_f) at different proportions of fines ψ.* ***(d-f)*** *Velocity results from experimental series A.* ***d*** *Velocity normalised by the maximum velocity achieved for 4 avalanches. Dashed horizontal line represents the location of the slope-break.* ***e*** *Velocity change during the acceleration and deceleration of phase 2.* ***f*** *Phase 3 average deceleration.*

395 deceleration of the material in phase 3 (fig. 6f) is not systematically reduced at low ψ between
396 0.10 and 0.35 (pore spaces not fully filled). At higher ψ, the average deceleration increases
397 throughout the range of ψ values.

398 **4.4 Volume**

399 Experiment series B (table 1) examines the combined effect of bidispersity and volume.
400 Bidispersity has the impact observed in series A also at the higher volume, increasing mobility
401 (runout and centre of mass displacement) at low ψ and progressively diminishing (fig. 7a).
402 However, fig. 7a illustrates that with higher volume, R_n values are greater. Nonetheless, R_{nCoM} is
403 not increased. This trend is confirmed by fig. 7b, illustrating H/R and H_{CoM}/R_{CoM}. Fig. 7c
404 suggests that spreading is greater for the higher volume avalanches.

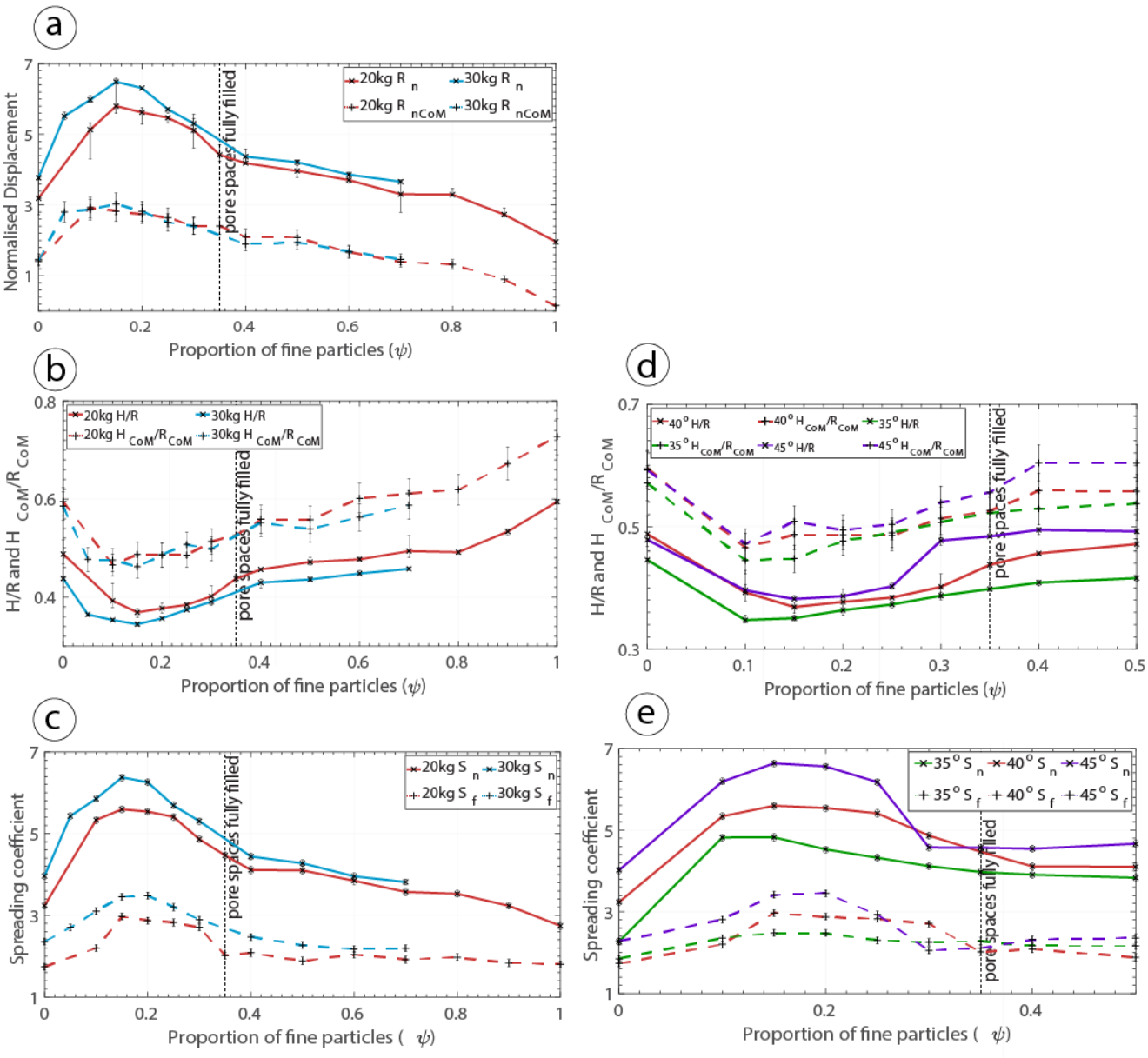

Figure 7 ***(a-c)*** *Results from experimental series B.* ***a*** *Frontal runout (R_n) and propagation of the centre of mass (R_n) at different proportions of fines (ψ).* ***b*** *H/R and H_{CoM}/R_{CoM} at different proportions of fines ψ.* ***c*** *Total spreading (S_n) and frontal spreading (S_f) at different proportions of fines ψ.* ***(d-e)*** *Results from experimental series C and D.* ***d*** *H/R and H_{CoM}/R_{CoM} at different proportions of fines ψ.* ***e*** *Total spreading (S_n) and frontal spreading (S_f) at different proportions of fines ψ.*

405

406 Volume does not systematically affect Vf in phase 1 in comparison to series A. In phase 2, at the
407 slope-break series B avalanches (lower volume) experienced similar deceleration on impact with
408 the slope-break series A. However, the acceleration of phase 2 achieves higher velocities and
409 lasts longer in higher volume avalanches (fig. 8).

In phase 3, pulses of acceleration and deceleration show a higher Vf amplitude in the higher volume avalanches. The V_{MAX} achieved in these pulses are greater at greater volumes. They are then decelerated and accelerated again to high velocities throughout phase 3 compared to the less voluminous series A (fig. 8).

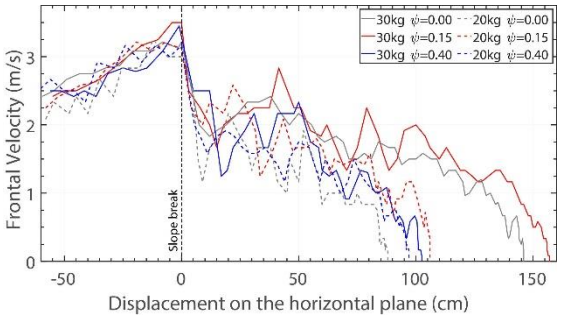

Figure 8 Frontal velocity comparison between the avalanches of series A (20kg) and B (30kg).

4.5 Inclination

For experiment series C and D (table 1) the slope inclination was 35° and 45° respectively, also altering the angle of the slope-break. The impact of the slope-break (fig. 1) is examined here, representing the transition between slopes and horizontal depositional surfaces of natural granular flows. By changing the inclination of the inclined slope the H, horizontal runout distance on the slope and height of the centre of mass prior to release are altered. For this reason, we use their H/R and H_{CoM}/R_{CoM} for comparison for series C and D (instead of R_n and R_{CoM}). Fig. 7d presents findings that suggest that between 35° and 45°, increased slope inclination generates less mobile avalanches, both in terms of their centre of mass as well as frontal runout. Although the maximum mobility of the centre of mass is achieved for all inclinations at ψ_{CRcom}=0.10, in the case of the maximum R a divergence is observed. The maximum is at ψ_{CRf}=0.15 for 40° and 45°, whereas it is at ψ_{CRf}=0.10 for 35°. Spreading also diverges as illustrated in fig. 7e. The effect of bidispersity on the degree of spreading is more intense at low ψ, before all pore spaces are filled. The 35° experiments achieve the lowest spreading, which is progressively increased at higher inclinations.

4.6 Size-ratio between particle species (Δ)

In experimental series E (table 1) the granular mixtures were composed of finer fine particles and coarser coarse particles, thus increasing the size ratio (Δ) between the two species (Δ= coarse particles mean diameter/fine particles mean diameter). Previous experimental series have a size ratio Δ=~17, whereas series E had a size ratio Δ=~45. Fig. 9a illustrates that increased Δ results in greater R_n and R_{nCoM} at low ψ. Fig. 9b, which also considers the difference in the centre of mass prior to release due to the difference in their sizes, confirms that at low ψ=0.05 and ψ=0.10 the granular mixture with greater Δ is more mobile in terms of R_n and R_{nCoM}. At ψ values greater than ψ>0.10, series E avalanches with greater Δ are less mobile. The peak in R_n and R_{nCoM} for experiment series E comes at ψ_{CRf}= ψ_{CRcom}=0.05, compared to ψ_{CRcom} =0.10 and ψ_{CRf}=0.15 for series A. In series E, spreading is greater for all ψ values when only the front of the deposit is considered (S_f) (fig. 9c). When the whole length of the deposit is considered (S_n), the spreading of flows from series A and E is very similar after the pore spaces between the coarse particles are filled by fines.

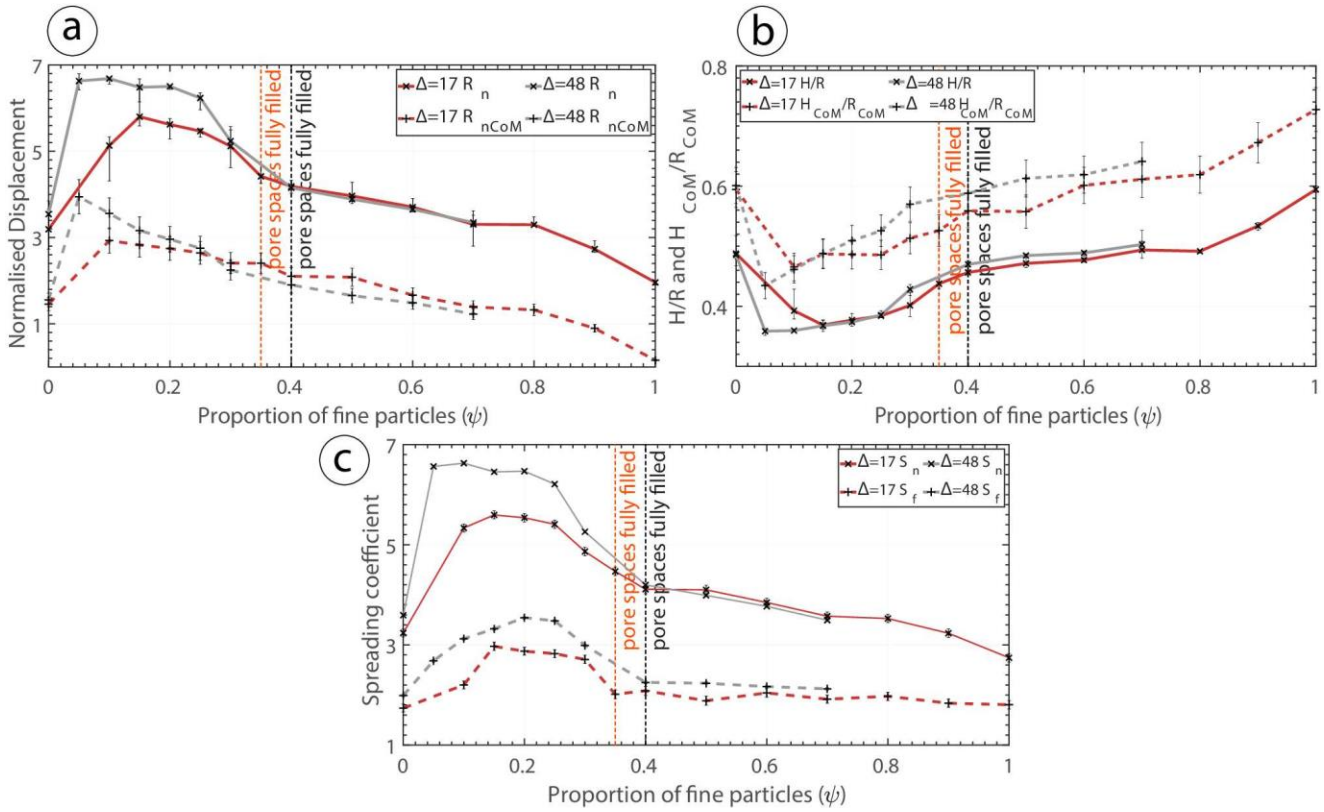

Figure 9 Results from experimental series E. ***a*** *Frontal runout (R_n) and propagation of the centre of mass (R_n) at different proportions of fines (ψ).* ***b*** *H/R and H_{CoM}/R_{CoM} at different proportions of fines ψ.* ***c*** *Total spreading (S_n) and frontal spreading (S_f) at different proportions of fines ψ.*

5. DISCUSSION

5.1 Deposit morphology observations

Rock/debris avalanches on flat valley floors generate horizontal runouts greater than the initial fall height (Hungr, 2002; Legros, 2002; McSaveney et al., 2000). This feature was recreated in the presented experiments with H/R values as low as 0.35. Although long-runout avalanches are difficult to recreate at the lab scale (Friedmann et al., 2006; Manzella and Labiouse, 2013), R_n values >6.5 have been achieved with bidisperse mixtures, compared to R_n=3.2-3.3 that is the maximum achieved by most monodisperse end-member avalanches. These values are in line with values exhibited by some natural rock/debris avalanches like the Elm (Switzerland) (R_n=5.1) and Frank (Canada) (R_n=5.6) rock avalanches. However, the appropriateness of such comparisons is discussed in the final section of the discussion.

Segregation of the size species is observed in the deposit in the vertical and longitudinal direction of the deposits (fig. 3a). This observation confirms that the effective composition of the flow is variable in time at different flow locations, while grading of the material and migration of fines to the base take place. When ψ increases, coarse particles are unable to travel independently, in agreement with what is observed by Phillips et al. (2006), as they are trapped in the mass of fine particles generating a sand-trap absorbing their kinetic energy (Bartali et al., 2020). Thus, coarse particles are observed deposited on top of the fine particles close to the slope-break (fig. 3a).

5.2 Frontal velocities during propagation

5.2.1 Phase 1

Phase 1 represents the propagation of the material under gravity (fig. 5 – panel 1). Vf is greater at greater slope inclinations because friction is reduced, and rolling is encouraged. Changes in ψ, volume and Δ do not have a systematic impact on Vf in this phase.

5.2.2 Phase 2

Velocity measurement and video observations support that the interaction of the avalanche with the slope-break causes loss of momentum (also observed by Crosta et al. 2017) and disorganisation in the particle position in the mass (fig. 5) (also observed by Manzella and Labiouse, 2009). The deceleration on initial contact with the horizontal plane is the result of increased friction due to the higher overburden stress at the change of direction of movement (Manzella and Labiouse, 2009; Yang et al., 2011). The deceleration is followed by acceleration as momentum is transferred by the rear of the flowing avalanche to the front (fig. 5 – panels 3-4). As the material at the front decelerates and transitions to a compressive regime, material still on

the slope interacts with them before they decelerate, pushing them forward, transferring energy and momentum (Hu et al., 2020; Longchamp et al., 2016).

5.2.3 Phase 3

Pulses of acceleration and deceleration of the front observed during propagation on the horizontal depositional surface (e.g. fig. 4, 6d, 8) have also been described by Van Gassen and Cruden (1989) and Bartali et al. (2015). Bartali et al. (2015) describe them as density waves travelling through the propagating mass generating stick-slip motion. Van Gassen and Cruden (1989) suggest that as the leading material decelerates due to friction, the approaching material from further back has not yet experienced equal retardation. It is therefore approaching at higher velocities than the material ahead. This leads to an interaction of momentum transfer between the particles at the avalanche front and the following material (Hu et al., 2021). The leading particles are propelled forward while the following material is decelerated to lower velocities or deposition. This process is referred to as energy transmission through impact by Van Gassen and Cruden (1989) and has also been reported through close videos examination of the experiments of Manzella and Labiouse (2009 - monodisperse) and Yang et al. (2011 – bidisperse/polydisperse). This can be observed by careful examination of the videos of the experiments of the current study. The cyclic recurrence of this process continues throughout the propagation and is evident through Vf oscillation pulses (fig. 8). Each subsequent pulse achieves lower velocities as the energy in the system decreases until the momentum and energy are depleted and the material is emplaced (Van Gassen and Cruden, 1989). By using energy equations to describe the momentum transfer occurring in these processes, Van Gassen and Cruden (1989) produced a model that suggests that a granular mass interacting in this manner results in significantly longer runouts (>1.5 times longer) than predicted by simple sliding block models with no momentum transfer. The transfer of momentum from the rear to the front causes the mass to spread and the front of the flow to travel farther (Legros, 2002; Manzella and Labiouse, 2009). The importance of spreading is addressed throughout the following discussion.

5.3 Fine particle content (ψ)

The findings are in agreement with previous studies reporting increased runout in granular avalanches composed of bidisperse mixtures compared to monodisperse (e.g. Phillips et al., 2006; Roche et al., 2006; Moro et al., 2010; Degaetano et al., 2013; Yang et al., 2015; Bartali et al., 2020). Maximum runouts are recorded at different proportions of ψ in different experiments as a function of parameters such as Δ and slope inclination. In experiment series A, R_n increases between ψ values of 0.0 and 0.15, and R_{nCoM} increases until ψ=0.10. In agreement to previous studies, it is observed that at low ψ fine particles segregate and position themselves at the bottom of the avalanche through kinetic sieving even if not initially positioned there, as also observed by

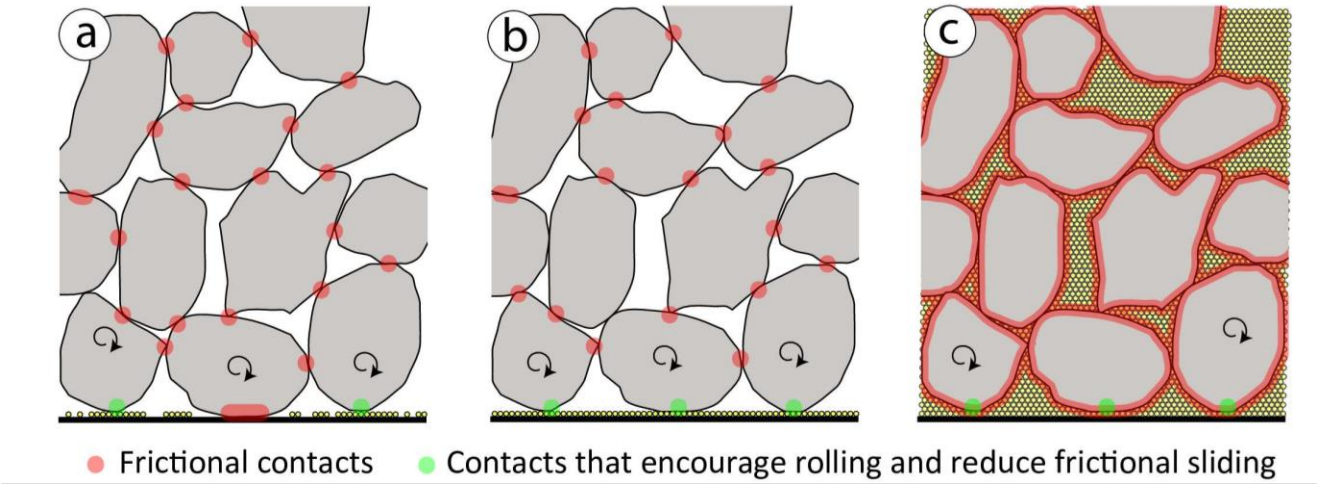

Figure 10 Types of contacts between the fine (yellow) and the coarse (grey) particles at different mixture proportions.

Phillips et al. (2006). Observations confirm the propositions of Goujon et al. (2007) that segregation is a very fast process in bidisperse mixtures at the scale of these experiments. Once at the base, the fine particles reduce frictional contact areas, acting as ball-bearers (e.g. Roche et al., 2006; Linares-Guerrero et al., 2007), and encourage rolling as opposed to frictional sliding (Phillips et al., 2006). This process reduces the friction coefficient at the base of the flow and inhibits frictional energy losses (Hu et al., 2021, 2020; Phillips et al., 2006). Consequently, the R_n and R_{nCoM} are increased. In series A, this process is most efficient at ψ=0.10 where maximum R_{nCoM} occurs (fig. 6a). At lower ψ values (<0.10), there are not enough fine particles to optimally lubricate all frictional contact surfaces at the base of the flow as not all coarse particles are supported by fines (fig. 10a) (Moro et al., 2010). The numerical modelling of Linares-Guerrero et al. (2007) suggests that the most efficient arrangement is one with a single grain size thickness layer continuous sheet of fines at the base of an avalanche. In such a case, the basal contacts are lubricated; but no particles are present within the avalanche body as illustrated in fig. 10b (Moro et al., 2010).

As ψ increases (>0.10), fines cover the base and start filling pore spaces between the coarse particles within the avalanche. Interparticle frictional contact surfaces increase as the pore spaces between the coarse particles are filled (fig. 10c). This progressively inhibits R_n and R_{nCoM} further with subsequent ψ increases as illustrated by fig. 6a, supporting the trend reported in other studies (Bartali et al., 2020; Hu et al., 2021, 2020; Moro et al., 2010; Phillips et al., 2006; Yang et al., 2011). The increased frictional losses in the interparticle contacts begin to offset the energy conserved at the base (Hu et al., 2020; Moro et al., 2010). However, it is important to note that even after all the pore spaces between coarse particles are filled ($0.35>\psi<0.80$ for series A), bidispersity enables mobilities greater than the monodisperse avalanches with all-coarse or all-fine particles (fig. 6a). This non-monotonic relationship between R_n and R_{nCoM} and ψ is reported

in similar bidisperse experiments (e.g. Phillips et al., 2006; Goujon et al., 2007; Moro et al., 2010; Yang et al., 2015).

The ψ_{CRf} has been suggested by various experimental studies to be between 0.05 and 0.50 (Appendix III) (Degaetano et al., 2013; Hu et al., 2020; Moro et al., 2010; Roche et al., 2006; Yang et al., 2015). In the current experiments, it is ψ_{CRf}=0.15 in the majority of cases; however, it changes to ψ_{CRf}=0.10 for the 35^{o} slope inclination (exp. series C) and ψ_{CRf}=0.05 for the experiments with greater Δ (exp. series E). Therefore, the findings suggest that ψ_{CRf} is a function of the geometry of the flow path and Δ, according to the parameters here examined.

The ψ affects the propagation of the centre of mass by basal lubrication. However, the spreading of the mass is affected in a process that appears to be independent as they do not follow the same trend (fig. 6, 7, 9). Greater runout does not necessarily imply greater propagation of the centre of mass. Therefore, ψ_{CRf} does not always coincide with ψ_{CRcom}. Investigating R_{CoM} reflects the energy dissipation of the flow and is therefore more appropriate for investigating the energetics of granular flows (Legros, 2002). In fact, H/R is mechanically irrelevant as a measure of mobility, since spreading can produce higher runouts irrespective of the centre of mass, and therefore kinetic energy dissipation (Davies, 1982; Dufresne et al., 2021; Legros, 2002). Thus, as initially suggested by Hsü (1975), the interpretation of the H/R (or *Fahrböschung*) as the friction angle is incorrect when considering energetics, and should instead be measured as the inclination of the line connecting the centre of gravity of the material pre-release and post-deposition (H_{CoM}/R_{CoM} or energy line gradient) (fig. 1b). In turn, H_{CoM}/R_{CoM} is not capable of considering the contribution of spreading to the runout (Davies, 1982; Davies and McSaveney, 1999). Therefore, a comparison of the two metrics, along with quantification of spreading, is needed to assess the impact and variability of spreading. Assessment of the spreading is a factor contributing to the runout.

Vf observations suggest that ψ affects the interaction of the avalanche with the slope-break (phase 2) and the subsequent propagation on the horizontal plane (phase 3). This is in agreement with the findings of the granular flow experiments of Fan et al. (2016) suggesting that material with different grain-size distributions produce different Vf during propagation. The findings of the current study suggest that small ψ values drastically lower phase 2 deceleration and the average deceleration rate of phase 3 compared to monodisperse endmembers (fig. 6 e, f). Fan et al. (2016) observed more pronounced decelerations in phase 2 in lower grain sizes. In accordance, the deceleration of the fine particles in phase 2 of the current experiments leads to accumulation of material at the toe of the slope. This is the result of the greater size ratio between particles and the slope-break discontinuity (Manzella and Labiouse, 2013). Furthermore, momentum transfer from the rear was not efficient at high ψ values as the accumulated fines acted as a sand-trap (Bartali et al., 2020; Fan et al., 2016). Nonetheless, the lower deceleration rate observed in phase 3 at ψ <0.7 (fig. 6f) supports that the addition of fine particles imposes a more efficient flow arrangement. The reduced frictional energy dissipation

they enable at the base makes more energy available as kinetic and reduces the deceleration of the material, generating longer runouts.

5.4 Volume

Examination of the H/R of natural events suggests that more voluminous rock/debris avalanches produce longer runouts (Shea and van Wyk de Vries, 2008). In the current experiments increased total volume (exp. series B) results in increased R_n (fig. 7a). However, in agreement with the monodisperse granular experiments of Manzella and Labiouse (2009), the increased R_f does not correspond to increased R_{CoM}. Examination of the avalanche spreading at different volumes in fig. 7c suggests that the greater R_n at higher volumes results from greater spreading. This results in a more spread, longer deposit even though the propagation of the centre of mass is similar (fig. 7). Spreading contributes the additional R_n, as also reported by Li et al. (2021) and Yang et al. (2011). Davies (1982) and Davies and McSaveney (1999) support that the long runouts of rock/debris avalanches is the result of spreading, rather than the mobility of the centre of mass exceeding what is predicted by simple frictional models. Field evidence rock/debris avalanche spreading is observed in Makris et al. (2023b). However, it has to be highlighted that both the mobility of the centre of mass and the spreading of the mass contribute to the overall runouts to a different extent under different conditions in the current experiments. In fact, rock/debris avalanche events have been suggested to have lower H_{CoM}/R_{CoM}, as well as H/R, to what is predicted by simple frictional models (Legros, 2002). While spreading contributes, to mass flow propagation, it is likely not the sole factor responsible for the high mobility.

The change in volume does not affect Vf during the propagation on the inclined plane and the deceleration part of phase 2. The divergence in Vf occurs with the initiation of momentum transfer from the rear to the front, in the acceleration stage of phase 2. At this stage, greater volumes generate greater momentum transfer resulting in greater acceleration for a longer time, as also reported by Manzella and Labiouse (2008). The greater Vf amplitude in phase 3 is due to greater pulses of momentum transfer between the front and the material behind. This is the result of the greater potential energy with higher volume, which is also more concentrated as a thicker flow with a lower proportion of the material in contact with the substrate. With greater volumes, and thus particle numbers, collisional opportunities also increase in constrained flows (Okura et al., 2000; Yang et al., 2011). Numerical modelling by Okura et al. (2000) supports that increased frequency of collisions could be a factor for longer runouts due to enhanced momentum transfer. This is proposed as the reason for the higher amplitude of the acceleration-deceleration pulses observed by Yang et al. (2011). These pulses propel the material at the front, enhancing spreading and R_n.

615 ### 5.5 Slope inclinations

616 Within the range of inclinations in these experiments (35^o – 45^o), higher inclinations lead to
617 greater spreading (fig. 7e), but lower H_{CoM}/R_{CoM} and H/R (fig. 7d). This is due to the interaction
618 of the avalanches with the slope-break. The impact of path irregularities on granular avalanche
619 propagation has been previously highlighted by researchers such as Heim (1932), Pudasaini et al.
620 (2005) and Manzella et al. (2013).

621 At higher inclinations, the S_f is greater at low ψ (0.1 – 0.3) (fig. 7e). The energy conserved due to
622 the lubrication of the base by the fines is transferred as momentum to the front of the flow
623 resulting in increased spreading. However, there is also loss of momentum between the particles
624 and the propagation surface, with energy lost outside the avalanche system. The slope-break
625 causes an increase in shear and loss of momentum (Crosta et al., 2017). The effect of a geometric
626 irregularity in the path of an avalanche on its mobility is a function of the size ratio between the
627 irregularity itself and the size of particles in the granular mass (Friedmann et al., 2006; Heim,
628 1932; Manzella et al., 2013). Increased slope angles generate a greater path irregularity and
629 energy dissipation (Manzella et al., 2013). The collision causes disorganisation in the particle
630 arrangement and momentum transfer, shifting the avalanche towards a more collisional regime
631 (Manzella and Labiouse, 2013), as observed in close examination of the lateral videos of the
632 experiments here described (fig. 5). However, the transfer of momentum decelerates the material
633 at the back limiting the overall kinetic energy acting in the propagation direction. Therefore, the
634 mobility of the centre of mass is reduced at higher inclinations with a steeper slope-break. This
635 leads to higher H/R and H_{CoM}/R_{CoM} for greater inclinations (fig. 7d). The increase in spreading is
636 offset by the lower $R_{CoM,}$ and consequently runouts are lower. At lower inclinations, there is less
637 disorganisation of the mass, fewer collisions and less momentum is transferred between particles.
638 Consequently, spreading is less, and its contribution to the overall runout is less important,
639 compared to the lubricating effect of bidispersity.

640

641 ### 5.6 Size ratio between particle species (Δ)

642 In experimental series E, where two granular materials with greater Δ are used, fines are more
643 effective at lubricating the avalanche at lower ψ. At ψ_{CRf} avalanches with higher Δ achieve
644 greater R_n (fig.9a). However, at greater ψ values (ψ>0.25) the R_{nCoM} is lower in the experiments
645 with higher Δ. This is the result of the smaller fine particles losing more energy at the slope-
646 break, suffering greater deceleration in phase 2 due to the greater size ratio between the grains
647 and the slope-break (Fan et al., 2016). Fine particles in sufficient quantities (ψ>0.25) can absorb
648 the momentum of coarser particles making the kinetic energy transfer in phase 2 less efficient. It
649 is likely that finer particles in mixtures with greater Δ are more efficient at limiting energy
650 dissipation by reducing frictional surfaces at the base or more effectively encouraging rolling.
651 However, in higher quantities, they inhibit mobility by acting as a sand-trap. Previous studies

have proposed that the mobility-enhancing effect of bidispersity is intensified with increased Δ (Bartali et al., 2020; Hu et al., 2020; Roche et al., 2006). In the bidisperse experiments of Goujon et al. (2007) avalanches with higher Δ resulted in more spread deposits with lower thickness compared to equivalent single-size end-members. In the bidisperse experiments of Hu et al. (2020) greatest R are exhibited by experiments with greater Δ. The value of ψ_{CR} is different in avalanches with different Δ in the current experiments. Duan et al. (2022) propose the existence of a correlation between the size of the particles and ψ_{CR}. However, a more systematic study is required to determine this relationship and the effect of Δ, as the results from the different studies are not consistent.

5.7 Scaling, granular flow regimes and kinetic sieving

Assessment of experimental scaling is essential in designing and evaluating the findings of granular avalanche experiments regarding their geomorphological and mechanical relevance to the dynamics of rock/debris avalanches (Iverson, 2015). Other than geometric scaling parameters, dynamic scaling parameters refer to the ratio between forces within the body of a granular avalanche and describe the evolving dynamics of the system (Iverson, 2015). Dynamic scaling parameters are crucial to ensure the similarity in conditions between experiments and real events. However, this scaling aspect of experimental design is very frequently overlooked (Iverson, 2015). Nonetheless, since the perfect correspondence between physical experiments and real events is not possible, some distorted scale effects are inevitably introduced (Heller, 2011). The potential scale-dependence of the simulated conditions must be assessed and is thus discussed in the subsequent sections.

5.7.1 Scaling of experiments

At the scale of these experiments, rolling motion at the base of the avalanche generates agitation and collisions between particles, leading to a collisional regime, as also described by Hu et al. (2021). The flow regime was initially qualitatively assessed in the current experiments through real-time observation and the videos. The collisional and frictional regimes, introduced by Drake (1990, 1991), describe a difference in the behaviour of propagating granular avalanches. In a frictional regime, the majority of the propagation particles are engaged in persistent frictional contacts, responsible for the majority of momentum transfer. In an avalanche under this regime the majority of the material propagates as a coherent plug over a basal agitated zone. Plug behaviour implies a coherent state, lacking agitation and propagating experiencing insignificant shear stresses. In contrast, in the collisional regime, the majority of momentum transfer is due to frequent particle collisions in an agitated mass with a high granular temperature. Different regimes and resultant granular behaviour (i.e. particle interaction frequency, duration etc.) alter the energy dissipated by avalanches and their mobility (Cagnoli and Piersanti, 2015).

Table 2 Experimental series A – Savage number, system-to-grain size ratio and information required for their calculation. (ψ: mess proportion of fines; δ: characteristic grain size diameter; T: avalanche thickness)

ψ	δ (m)	Volume (m³)	T (m)	System-to-grain size ratio	Savage number
0.00	0.0128	0.0168	0.06	1.1E+04	0.773
0.10	0.0116	0.0157	0.057	1.4E+04	0.740
0.15	0.0110	0.0152	0.054	1.6E+04	0.782
0.20	0.0104	0.0148	0.055	1.9E+04	0.662
0.25	0.0098	0.0145	0.051	2.2E+04	0.736
0.30	0.0092	0.01388	0.055	2.6E+04	0.517
0.35	0.0086	0.0128	0.051	2.9E+04	0.566
0.40	0.0080	0.0115	0.0483	3.2E+04	0.576
0.50	0.0068	0.0109	0.045	5.0E+04	0.514
0.60	0.0056	0.0123	0.051	1.0E+05	0.239
0.70	0.0044	0.0137	0.051	2.4E+05	0.147
0.80	0.0032	0.0141	0.063	6.4E+05	0.041
0.90	0.0020	0.0132	0.0645	2.5E+06	0.015
1.00	0.0008	0.0133	0.03	4.5E+07	0.021

The Savage number (N_{Sa}) is the ratio between particle collision stress and the load on the bed due to the weight of particles and can be approximated as (Iverson, 1997; Iverson et al., 2004):

$$N_{Sa} \approx \frac{u^2 \delta^2}{g T^3}$$

Eq. (4)

where u is the maximum speed (ms^{-1}), δ is the typical grain diameter (m), g is the gravitational acceleration (ms^{-2}) and T is the avalanche thickness. The typical grain diameter is characterised as the mean particle diameter D_{43} (Breard et al., 2020; Gu et al., 2016), calculated as the volume average mean diameter:

$$D_{43} = n_q d_q$$

Eq (5)

where n_q is the mass fraction of a particle class q with diameter d_q. The N_{Sa} is a non-dimensional characterisation of the flow regime, differentiating between the frictional and collisional regime by quantifying the relative importance of inertial stresses over the total stresses in steady, gravity-driven flows with free upper surfaces (Hsu et al., 2014; Savage, 1984). When the N_{Sa} is larger than 0.1, the regime is collisional with significant collisional stresses (Hsu et al., 2014; Iverson, 2015; Iverson and Vallance, 2001). Greater N_{Sa} values imply increasing particle collisions. Conversely, when N_{Sa} is smaller than 0.1, the regime is frictional and friction-

dominated (Iverson and Vallance, 2001; Savage and Hutter, 1989). The N_{Sa} quantifies this ratio independent of scale (Iverson, 1997).

Two important factors for the N_{Sa} are the typical grain diameter δ and avalanche thickness T (Eq. 4). The flume tests of Cagnoli and Romano (2012) and Cagnoli and Piersanti (2015) suggest that changes in the mobility of small-scale granular avalanches triggered by grain size and volume changes are, in fact, due to the resultant variation of granular agitation and the N_{Sa}. The agitation and nature of particle interactions is a principal factor for energy dissipation and should be considered when interpreting avalanches (Li et al., 2021). Indeed, avalanches in this study with different ψ (table 2) have variable δ and T, according to the proportion of each particle size species. For experimental series A, the N_{Sa} was calculated for their propagation on the horizontal plane after the slope-break. For the majority of the experiments, the N_{Sa} is above 0.1 (fig. 11a), confirming that the material propagated under a collisional regime which is not representative of rock/debris avalanches (table 2). For experimental series A, only experiments with ψ>0.80 result in N_{Sa} values in the frictional regime (fig. 11a).

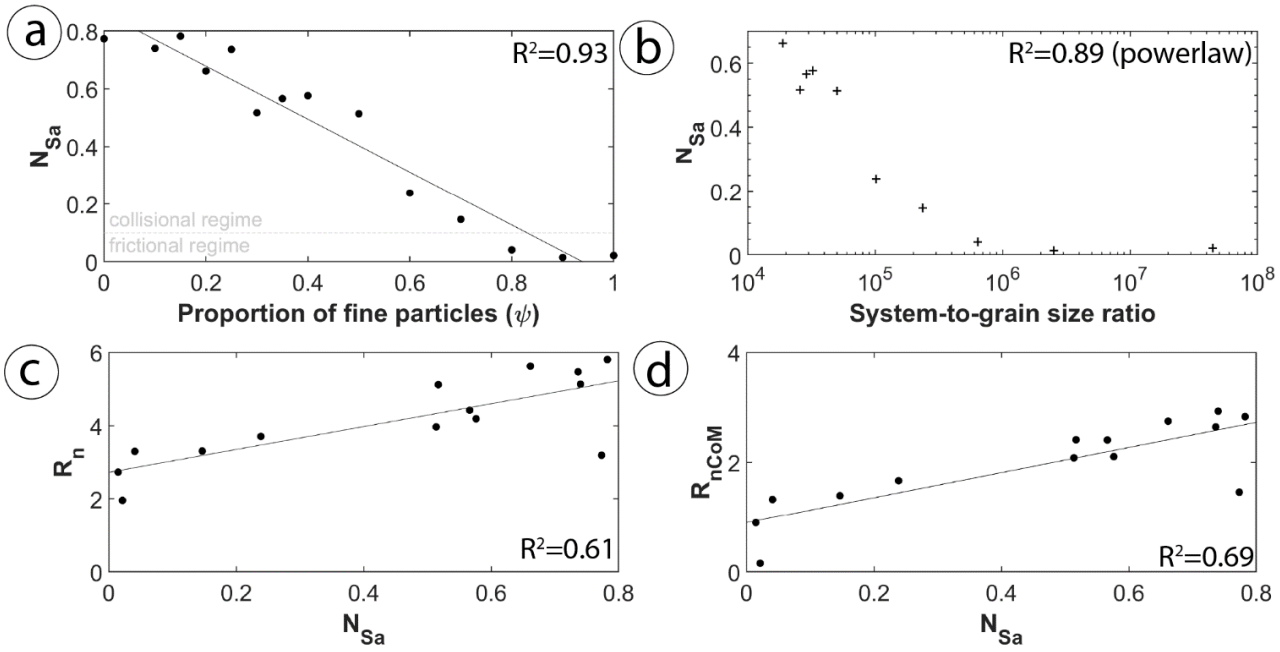

Figure 11 Scaling evaluation of experimental series A. ***a*** *N_{Sa} as a function of ψ.* ***b*** *N_{Sa} as a function of the system-to-grain size ratio.* ***c*** *R_n as a function of N_{Sa}.* ***d*** *R_{nCoM} as a function of N_{Sa}*

The T component of the N_{Sa} equation is directly correlated to the number of particles in an avalanche (assuming equal δ). The system-to-grain size ratio proposed by Cabrera and Estrada (2021) is essentially a proxy for the number of particles in a granular system. The ratio is here defined as the ratio of the volume occupied in the mass by a single particle of mean diameter

when assuming spherical particles arranged in simple cubic packing to the total volume of material:

$$\text{system} - \text{to} - \text{grain size ratio} = \frac{V}{4\sqrt{2}\left(\frac{\delta}{2}\right)^3} \qquad Eq\ (\ 6\ )$$

The system-to-grain size ratio of the presented experiments is similar to the experiments previously mentioned (Appendix I). Li et al. (2021) support that larger grain sizes/smaller volumes (i.e., smaller system-to-grain size ratio) increase collisions, the granular temperature and the N_{Sa}. The findings of this study also support a negative correlation between the system-to-grain size ratio and the N_{Sa} in experimental series A (fig. 11b). Li et al. (2021) find that increasing the volume and decreasing δ have the same effect since they both affect the system-to-grain size ratio. The findings of Cabrera and Estrada (2021) support that with sufficiently large system-to-grain-size ratios (expected in natural avalanches) the mobility and shear strength of granular column collapses is independent of grain-size distribution variations. As granular systems become larger, grain size effects weaken (Cabrera and Estrada, 2021). Consequently, small system behaviour can be biased by small system-to-grain size ratios and flow height, resulting in high N_{Sa} values and energy exchange dominated by collisions. Such conditions are unrepresentative of natural processes (Cabrera and Estrada, 2021; Li et al., 2021). With small numbers of particles, agitation is greater per unit of flow mass since agitation is able to propagate up from the base and agitate a higher proportion of the avalanche (Cagnoli and Romano, 2012, 2010). Li et al. (2021) observe that a reduction of δ or increase in volume leads to localisation and magnification of shear stress at the base of the avalanche, leaving the overriding material to travel as a plug with no agitation. This is also observed in numerical simulations of granular avalanches (e.g. Walton, 1993; Silbert et al., 2001). The N_{Sa} of the plug is zero, resulting in extremely low overall N_{Sa} values for such avalanches (Li et al., 2021).

Small system-to-grain size ratios can lead to behaviours unrepresentative of large-scale events due to the small number of particles involved in the experimental systems (grain size effect), rather than the grain-size composition and distribution (Cabrera and Estrada, 2021, 2019; Li et al., 2021). The increase in the R_n and R_{CoM} observed in avalanches from this study exhibit a correlation with the N_{Sa} (fig. 11c, d). The correlation suggests that the difference might be correlated to the alteration of the N_{Sa} and the collisional regime, instead of ψ being the exclusive factor.

Therefore, to achieve geomorphological and mechanical relevance experiments of rock/debris avalanches require scales which are large enough (number of particles/avalanche thickness) to permit a frictional regime behaviour (Iverson, 2015). High N_{Sa} values and the observation of collisional behaviour is very frequent in the reporting of lab-scale granular avalanche experiments. Li et al. (2021) calculate and report that N_{Sa} values of their experiments reflect a frictional regime for the majority of their experimental conditions. However, in the experiments of Cagnoli and Romano (2012), N_{Sa} is reported to have been larger than the threshold of 0.1. Lai et al. (2017), Bartali et al. (2020) and Duan et al. (2022) report their qualitative observation of

767 collisional behaviour without further examining or commenting on the implications of this
768 behaviour to the comparison with natural events.

769 The estimated N_{Sa} values of natural rock/debris avalanches are typically much lower than 0.1
770 (data collected and presented in Appendix Table 2 of Li et al. 2021). A uniform collisional
771 regime does not occur in natural events and thus values of shear stresses are dissimilar to small-
772 scale avalanches (Iverson et al, 2004). When N_{Sa} is high, grain collision stresses have a higher
773 importance in the flow (Savage and Hutter, 1989). As highlighted by Duan et al. (2022), in a
774 collisional regime the energy-transferring collisions and the expansion of the mass are enhanced.
775 Therefore, the current experiments, as well as a large part of lab-scale granular avalanche
776 experiments, occur in the collisional regime. The flow regime, dynamics and shear stresses
777 observed are scale-dependent.

778

779 ### *5.7.2 Granular avalanche propagation processes comparison at different scales*

780 As observed in the current experiments, in small free-surface avalanches composed of binary
781 mixtures the finer particles percolate to the to generate size segregation. Increased mobility
782 requires fine particles at the base of the flow, between coarse particles and the substrate. The
783 segregation process is essential to permit bidispersity to enhance mobility. Dispersive pressure
784 has been proposed as a mechanism potentially enabling size segregation in natural granular
785 avalanches (Bagnold, 1954; Cruden and Hungr, 1986). However, this would require a density
786 difference between different sizes which is not consistent with natural material (Legros, 2002).
787 In the current experiments, the process that generates the segregation is kinetic sieving. The
788 granular mass dilates during the agitated motion with voids opening between the coarse particles
789 for the finer ones to percolate through to the base due to gravity (Savage and Lun, 1988). Hu et
790 al. (2021) propose that this process takes place throughout the body of a granular avalanche,
791 leading to inverse grading. They argue that similarly to lab experiments, kinetic sieving allows
792 fine particles to migrate to the base and lubricate rock/debris avalanches. This is based on the
793 idea, prevalent in the past, where rock/debris avalanches were envisaged as rapid granular flows
794 with their dynamics dominated by chaotic and energetic particle collisions (De Blasio 2011).
795 Accordingly, some researchers have suggested that rock/debris avalanches are efficient at sorting
796 particles by size (e.g. Savage and Lun, 1988). This would lead to inverse grading observed
797 across deposits (Cruden and Hungr, 1986; Dufresne, 2009; Hungr and Evans, 2004; Middleton,
798 1976). Although some studies do report grading at the deposit scale (e.g. Hewitt, 1998; Crosta et
799 al., 2007), others observe the lack of it (e.g. Shreve, 1966; McSaveney, 1978; Schilirò et al.,
800 2019; Makris et al., 2023a). More recent work supports that grading is a bias introduced by the
801 presence of a coarse carapace at the top of rock avalanche deposits and does not persist lower in
802 their body (Dufresne and Dunning, 2017; Dunning, 2006; Dunning and Armitage, 2011).
803 Grading is not generally observed in deposits and it is no longer believed that flows are
804 dominated by chaotic particle collisions and high granular temperatures (e.g. Dunning, 2006;
805 Dufresne et al., 2016; Makris et al., 2020, 2023a, 2023b; Paguican et al., 2021).

Schilirò et al. (2019) propose the existence of dimensional limits for kinetic sieving. They propose a threshold in flow velocity and particle number/flow thickness over which a collisional regime is not attainable. Above the critical thickness value and below a critical velocity a flow develops an agitated basal layer with the areas above travelling as a plug (frictional regime). Agitation throughout the material is essential for kinetic sieving, and in the lack of it, segregation is not possible. The hypothesis of bidispersity increasing mobility by acting to increase rotation and decreasing frictional areas at the base necessitates inverse grading. However, the low threshold velocity and high particle numbers required to allow the agitation and segregation are unrealistically far from the values for the velocities and the thickness of natural rock/debris avalanches as explained by Schilirò et al. (2019). Sedimentological observations are in agreement with the lack of grading observed and offer support for the existence of the dimensional limit for kinetic sieving. Bidispersity is observed in the grain-size distribution of rock/debris avalanches, however, kinetic sieving is not capable of imposing segregation, which as the experiments suggest is vital for enhancing mobility. Additionally, an agitated basal layer composed of the fine particles would not be capable of supporting a rocky slab plug at the scale of rock/debris avalanches for realistic values of the coefficient of restitution and propagation angles of real events according to the force balance calculations of De Blasio and Elverhøi (2008). This bidispersity mechanism can therefore be excluded as a friction-reducing mechanism at the scale of rock/debris avalanches.

5.7.3 Implications for rock/debris avalanches:

Small-scale experiments are not capable of reproducing some of the processes enabled at the scale of natural geophysical flows (Iverson et al., 2004). Naturally, laboratory experiments cannot simulate fragmentation processes due to the low energies in the system as an example (Bowman et al., 2012; De Blasio and Crosta, 2014). Likewise, the seismicity of the event cannot be simulated (Davies and McSaveney, 1999). Even so, if fluid effects are negligible, major features of rock/debris avalanches can still be reproduced by analogue experiments with appropriate scaling since their dynamics are principally controlled by the internal and basal friction coefficients and the interaction of the avalanche with its path (Davies and McSaveney, 1999; Dufresne, 2012; Iverson et al., 2004; Iverson and Denlinger, 2001; Yang et al., 2011). However, scepticism regarding the effectiveness of small-scale experiments centres around their being too brief, idealised and restricted by initial conditions and artificial boundaries to represent the vast complexities of natural geophysical processes (e.g. Baker, 1996). Iverson (2015) caution that the geomorphological relevance of small-scale granular flow experiments carried out in the past decades (e.g. Iverson et al., 2004; Pudasaini and Hutter, 2007; Mangeney et al., 2010) should be critically evaluated, in terms of scaling and interpretation in comparison to natural processes, before being extended to direct comparison with natural phenomena.

To highlight the distorted scale effects, the '*Scheidegger*' plot (H/R plotted against volume) of all the experimental avalanches of this study is compared to a rock/debris avalanche inventory

(fig. 12). The relationship between the H/R and volume can be reasonably described by a power law (Scheidegger, 1973). Regression illustrates a relationship; albeit with wide dispersion increasing the degree of uncertainty ($0.36< R^2 <0.63$, Shea and van Wyk de Vries 2008). Data dispersion, partially mitigated by the log scale, constitutes the comparison of such trends inherently problematic. Nonetheless, the findings from the current experiments plotted in the same area in fig. 12 suggest that they do not follow the same relationship. They produce H/R values equivalent to some events, but with considerably smaller volumes, suggesting that the processes involved are scale-dependent and non-equivalent.

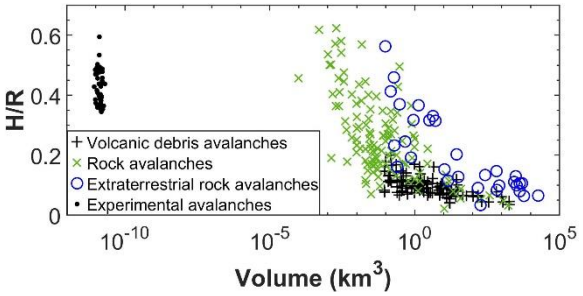

Figure 12 Apparent coefficient of friction (H/R) versus volume for volcanic debris avalanches, rock avalanches and extraterrestrial rock avalanches (from Makris (2020) modified after van Wyk de Vries and Delcamp (2015) and Hürlimann and Ledesma (2003) in comparison to the experimental avalanches of the current study.

Caution and a rigorous approach are crucial in their design and the interpretation of analogue experiment results (Iverson, 2015). Geomorphological and mechanical relevance should not be assumed on the basis of superficial or morphometric similarity, as it does not necessarily imply similarity in processes as exemplified here (Iverson, 2015). Dynamic scaling analysis must become a standard procedure in designing and interpreting analogue granular avalanche experiments to ensure the effectiveness of the experiments in examining the desired processes and dynamics.

The hypothesis of a basal low friction zone, with a potentially bidisperse grain-size distribution supporting the weight of a plug above it, is also disputed by the observation of shear zones throughout the body of rock/debris avalanche deposits at various depths (e.g. Roverato et al., 2015; Dufresne et al., 2016; Dufresne and Dunning, 2017; Wang et al., 2019; Hughes et al., 2020; Makris et al., 2023). The shear zones confirm that shear is not exclusively accommodated at the base (Dufresne and Dunning, 2017). Shear zones are also characterised by bidisperse distributions according to the observations of Dufresne and Dunning (2017). Therefore, their bidisperse grain-size distribution could potentially constitute a more efficient network for the accommodation of shear stress. According to the multislide plug flow model (Paguican et al., 2021; Roverato et al., 2015), shear zones can efficiently accommodate shear within the body of the avalanche. Indeed, frictionites have been reported within shear zones in the body of the Köfels rockslide supporting that they represent areas of shear concentration (Dufresne and Dunning, 2017). Therefore, it is plausible that in large volumes, the multi-slide plug flow could

potentially accommodate multiple levels of plugs supported above shear zones. In this case, agitation and a segregation mechanism are not required as bidispersity can be generated in situ. These shear zones are similar to the distributed stress fluidisation model proposed by Makris et al. (2023a), however they are potentially more stable and continuously active during the propagation. Experimental findings suggest that bidisperse distributions are generated with increased shear or confining pressures (Caballero et al., 2014; Iverson et al., 1996) either by fine particles generated through shearing or the preservation of larger survivor clasts through the preferential comminution of smaller particles around them (Dufresne and Dunning, 2017; Makris et al., 2020). Shear zones potentially focus shear stresses and act as corridors that localise shear accommodation around more coherent domains that are less exposed to shear and thus lacking agitation dissipate less energy (Crosta et al., 2007; Li et al., 2021; Paguican et al., 2021; Roverato et al., 2015). Therefore, only a small proportion of the propagating mass is engaged in high energy dissipation motion (Li et al., 2021). The analogue experiments of Li et al. (2021) and numerical simulations of Lai et al. (2017) support the assumption that the material above such areas of shear localisation can be transported as a plug. If the bidisperse grain-size distribution can inhibit frictional energy losses, more energy would be available for kinetic energy and the propagation of the mass, effectively reducing the apparent friction angle. Most importantly, this theory is consistent with the geomorphic and sedimentological features of deposits. However, the multiple plug flow hypothesis aided by bidisperse grain-size distribution requires a more detailed and systematic evaluation.

6. CONCLUSIONS

Analogue granular flow experiments were carried out in a scaled setup to investigate the effects of bidispersity on granular avalanche propagation processes and dynamics. Analysis of the findings leads to the following conclusions:

- Bidispersity has the potential to affect energy dissipation in granular avalanches and increase their runout, at the scale of the considered experimental conditions. It was found that low ψ values between ψ=0.05 and ψ=0.15 (depending on experimental conditions) are most efficient at enhancing mobility. At higher ψ values, up to ψ=0.80, the mobility is still greater than ψ=0.00.
- The effect of bidispersity is altered according to the inclination of the slope before the horizontal depositional surface. However, it is not affected by the volume of the material. Spreading is also affected by the inclination of the slope before the horizontal depositional surface and the angle of the slope-break. Increases in runout with increased volumes are the result of enhanced spreading. Runout is affected by both the displacement of the centre of mass as well as the spreading of the mass.
- A slope-break generates disorganisation of the mass, loss of momentum, and increase of collisions that transfer momentum from the back of the avalanche to the front.
- At low ψ, increased Δ is more effective at increasing mobility, resulting in longer runouts. However, the finer particles lose more energy at the slope-break due to the greater size ratio between them and the path irregularity. When present at higher

915 quantities their earlier deposition acts as a sand-trap for the coarser particles and reduces
916 runout.
917 • The increase in mobility due to bidispersity is the effect of fines at the base of the flow,
918 between coarse particles and the propagation surface, limiting frictional surfaces and
919 encouraging rolling. This study suggests that this process requires size segregation by
920 kinetic sieving. The occurrence of this process in small-scale experiments is scale-
921 dependent and does not occur at the scale of natural rock/debris avalanches. Therefore,
922 bidispersity is unlikely to enhance the mobility of rock/debris avalanches by providing a
923 more efficient shearing arrangement at their base.
924 • This study highlights that dynamic scaling analysis must become a standard procedure in
925 designing and interpreting analogue granular avalanche experiments.
926

927 *List of abbreviations*

R	horizontal runout of the front of the avalanche from the front of the material pre-release
R_{hCoM}	propagation of the centre of mass on the horizontal plane
R_{CoM}	horizontal propagation distance of the centre of mass
R_f	frontal runout on the horizontal plane
R_n	normalised frontal runout on the horizontal plane
R_{nCoM}	normalised propagation of the centre of mass on the horizontal plane
ψ	proportion of fines
ψ_{CRf}	critical proportion of fines for maximum frontal runout
ψ_{CRcom}	critical proportion of fines for maximum propagation of the centre of mass
Vf	frontal velocity
H	maximum fall height
H_{CoM}	vertical difference between the location of the centre of mass in the box and in the final deposit
V	volume
h*	$= V^{1/3}$
S_n	total spreading
S_f	frontal spreading
L	deposit length
Δ	size ratio between coarse and fine particles
V_{MAX}	maximum velocity in phase 2
N_{Sa}	Savage number
δ	typical grain diameter (m)
g	gravitational acceleration (ms^{-2})
T	avalanche thickness

928

Acknowledgments

This work was funded by the university of Plymouth through a University of Plymouth Studentship (URS) to Symeon Makris. The authors would like to thank Amelia Dunn, Georgina White, Taylor Wood and Jack Collingbridge who carried out part of the experiments as part of their undergraduate dissertations for the University of Plymouth in 2020-2021.

Open Research

Experimental results, 3D reconstruction of deposits and video footage of the experiments can be made available by Symeon Makris (makris.symeon@gmail.com) upon request by interested readers.

References

Ahmadipur, A., Qiu, T., Sheikh, B., 2019. Investigation of basal friction effects on impact force from a granular sliding mass to a rigid obstruction. Landslides 1089–1105. https://doi.org/10.1007/s10346-019-01156-0

Bagnold, R.A., 1954. Experiments on a gravity-free dispersion of large solid spheres in a Newtonian fluid under shear. Proc. R. Soc. London. Ser. A. Math. Phys. Sci. 225, 49–63. https://doi.org/10.1098/rspa.1954.0186

Baker, V.R., 1996. Hypotheses and geomorphological reasoning, in: Rhoads, B.L., Thorn, C.E. (Eds.), The Scientific Nature of Geomorphology. Wiley, New York, pp. 57–85.

Banton, J., Villard, P., Jongmans, D., Scavia, C., 2009. Two-dimensional discrete element models of debris avalanches: Parameterization and the reproducibility of experimental results. J. Geophys. Res. Earth Surf. 114, 1–15. https://doi.org/10.1029/2008JF001161

Bartali, R., Rodríguez Liñán, G.M., Torres-Cisneros, L.A., Pérez-Ángel, G., Nahmad-Molinari, Y., 2020. Runout transition and clustering instability observed in binary-mixture avalanche deposits. Granul. Matter 22. https://doi.org/10.1007/s10035-019-0989-0

Bartali, R., Sarocchi, D., Nahmad-Molinari, Y., 2015. Stick-slip motion and high speed ejecta in granular avalanches detected through a multi-sensors flume. Eng. Geol. 195, 248–257. https://doi.org/10.1016/j.enggeo.2015.06.019

Bernard, K., Thouret, J.C., van Wyk de Vries, B., 2017. Emplacement and transformations of volcanic debris avalanches-A case study at El Misti volcano, Peru. J. Volcanol. Geotherm. Res. 340, 68–91. https://doi.org/10.1016/j.jvolgeores.2017.04.009

Bernard, K., van Wyk de Vries, B., 2017. Volcanic avalanche fault zone with pseudotachylite and gouge in French Massif Central. J. Volcanol. Geotherm. Res. 347, 112–135.

https://doi.org/10.1016/j.jvolgeores.2017.09.006
Bowman, E.T., Take, W.A., Rait, K.L., Hann, C., 2012. Physical models of rock avalanche spreading behaviour with dynamic fragmentation. Can. Geotech. J. 49, 460–476. https://doi.org/10.1139/T2012-007
Breard, E.C.P., Dufek, J., Fullard, L., Carrara, A., 2020. The Basal Friction Coefficient of Granular Flows With and Without Excess Pore Pressure: Implications for Pyroclastic Density Currents, Water-Rich Debris Flows, and Rock and Submarine Avalanches. J. Geophys. Res. Solid Earth 125, 1–22. https://doi.org/10.1029/2020JB020203
Caballero, L., Sarocchi, D., Soto, E., Borselli, L., 2014. Rheological changes induced by clastfragmentation in debrisflows. J. Geophys. Res. Earth Surf. 119, 1800–1817. https://doi.org/10.1002/2013JF002871.Received
Cabrera, M., Estrada, N., 2021. Is the Grain Size Distribution a Key Parameter for Explaining the Long Runout of Granular Avalanches? J. Geophys. Res. Solid Earth 126, 1–9. https://doi.org/10.1029/2021JB022589
Cabrera, M., Estrada, N., 2019. Granular column collapse: Analysis of grain-size effects. Phys. Rev. E 99, 1–7. https://doi.org/10.1103/PhysRevE.99.012905
Cagnoli, B., Piersanti, A., 2015. Grain size and flow volume effects on granular flow mobility in numerical simulations: 3-D discrete element modeling of flows of angular rock fragments. J. Geophys. Res. Solid Earth 3782–3803. https://doi.org/10.1002/2015JB012608.
Cagnoli, B., Romano, G.P., 2012. Effects of flow volume and grain size on mobility of dry granular flows of angular rock fragments: A functional relationship of scaling parameters. J. Geophys. Res. Solid Earth 117, 1–13. https://doi.org/10.1029/2011JB008926
Cagnoli, B., Romano, G.P., 2010. Effect of grain size on mobility of dry granular flows of angular rock fragments: An experimental determination. J. Volcanol. Geotherm. Res. 193, 18–24. https://doi.org/10.1016/j.jvolgeores.2010.03.003
Campbell, C.S., 1990. Rapid granular flows. Annu. Rev. Fluid Mech. 22, 57–90.
Collins, G.S., Melosh, H.J., 2003. Acoustic fluidization and the extraordinary mobility of sturzstroms. J. Geophys. Res. Solid Earth 108, 1–14. https://doi.org/10.1029/2003jb002465
Crosta, G.B., De Blasio, F.V., De Caro, M., Volpi, G., Imposimato, S., Roddeman, D., 2017. Modes of propagation and deposition of granular flows onto an erodible substrate: experimental, analytical, and numerical study. Landslides. https://doi.org/10.1007/s10346-016-0697-3
Crosta, G.B., Frattini, P., Fusi, N., 2007. Fragmentation in the Val Pola rock avalanche, Italian Alps. J. Geophys. Res. Earth Surf. 112, 1–23. https://doi.org/10.1029/2005JF000455
Cruden, D., Hungr, O., 1986. The debris of the Frank Slide and theories of rockslide–avalanche mobility. Can. J. Earth Sci. 23, 425–432. https://doi.org/10.1139/e86-044
Davies, T., 1982. Spreading of rock avalanche debris by mechanical fluidization. Rock Mech. 24, 9–24.
Davies, T., McSaveney, M., 2012. Mobility of long-runout rock avalanches. Landslides–types, Mech. Model. Ed. by JJ Clague D. Stead. 50–58.
Davies, T., McSaveney, M.J., 1999. Runout of dry granular avalanches. Can. Geotech. J. https://doi.org/10.1139/t98-108
De Blasio, F.V., 2011. Introduction to the Physics of Landslides, Introduction to the Physics of Landslides. https://doi.org/10.1007/978-94-007-1122-8
De Blasio, F.V., Crosta, G.B., 2014. Simple physical model for the fragmentation of rock avalanches. Acta Mech. 225, 243–252. https://doi.org/10.1007/s00707-013-0942-y

De Blasio, F.V., Elverhøi, A., 2008. A model for frictional melt production beneath large rock avalanches. J. Geophys. Res. Earth Surf. 113, 1–13. https://doi.org/10.1029/2007JF000867

Degaetano, M., Lacaze, L., Phillips, J.C., 2013. The influence of localised size reorganisation on short-duration bidispersed granular flows. Eur. Phys. J. E 36. https://doi.org/10.1140/epje/i2013-13036-9

Denlinger, R.P., Iverson, R., 2001. Flow of variably fluidized granular masses across three-dimensional terrain: 2. Numerical predictions and experimental tests. J. Geophys. Res. Solid Earth 106, 537–552. https://doi.org/10.1029/2000JB900329

Drake, T.G., 1991. Granular flow physical experiments and their implications for microstructural theories. J. Fluid Mech. https://doi.org/10.1017/S0022112091001994

Drake, T.G., 1990. Structural features in granular flows. J. Geophys. Res. Solid Earth 95, 8681–8696.

Duan, Z., Wu, Y. Bin, Peng, J.B., Xue, S.Z., 2022. Characteristics of sand avalanche motion and deposition influenced by proportion of fine particles. Acta Geotech. 0123456789. https://doi.org/10.1007/s11440-022-01653-y

Dufresne, A., 2012. Granular flow experiments on the interaction with stationary runout path materials and comparison to rock avalanche events. Earth Surf. Process. Landforms 37, 1527–1541. https://doi.org/10.1002/esp.3296

Dufresne, A., 2009. Influence of runout path material on rock and debris avalanche mobility: field evidence and analogue modelling . Sci. York 268.

Dufresne, A., Bösmeier, A., Prager, C., 2016. Sedimentology of rock avalanche deposits – Case study and review. Earth-Science Rev. 163, 234–259. https://doi.org/10.1016/j.earscirev.2016.10.002

Dufresne, A., Davies, T., 2009. Longitudinal ridges in mass movement deposits. Geomorphology 105, 171–181. https://doi.org/10.1016/j.geomorph.2008.09.009

Dufresne, A., Dunning, S., 2017. Process dependence of grain size distributions in rock avalanche deposits. Landslides 14, 1555–1563. https://doi.org/10.1007/s10346-017-0806-y

Dufresne, A., Siebert, L., Bernard, B., 2021. Distribution and geometric parameters of volcanic debris avalanche deposits, in: Volcanic Debris Avalanches. Springer, pp. 75–90.

Dunning, S., 2006. The grain-size distribution of rock avalanche deposits in valley-confined settings. Ital. J. Eng. Geol. Environ. 1, 117–121. https://doi.org/10.4408/IJEGE.2006-01.S-15

Dunning, S., Armitage, P.J., 2011. The Grain-Size Distribution of Rock-Avalanche Deposits: Implications for Natural Dam Stability, in: Natural and Artificial Rockslide Dams. Springer, Berlin, Heidenberg, pp. 479–498. https://doi.org/10.1007/978-3-642-04764-0

Fan, X., Tian, S., Zhang, Y., 2016. Mass-front velocity of dry granular flows influenced by the angle of the slope to the runout plane and particle size gradation. J. Mt. Sci. 13, 234–245.

Friedmann, S.J., Taberlet, N., Losert, W., 2006. Rock-avalanche dynamics: Insights from granular physics experiments. Int. J. Earth Sci. 95, 911–919. https://doi.org/10.1007/s00531-006-0067-9

Glicken, H., 1996. Rockslide-debris avalanche of May 18, 1980, Mount St. Helens volcano, Washington. USGS Open File Report 96-677. Bull. Surv.

Goujon, C., Dalloz-Dubrujeaud, B., Thomas, N., 2007. Bidisperse granular avalanches on inclined planes: A rich variety of behaviors. Eur. Phys. J. E 23, 199–215. https://doi.org/10.1140/epje/i2006-10175-0

Gu, Y., Ozel, A., Sundaresan, S., 2016. Rheology of granular materials with size distributions

across dense-flow regimes. Powder Technol. 295, 322–329. https://doi.org/10.1016/j.powtec.2016.03.035
Heim, A., 1932. Bergsturz und menschenleben. Fretz & Wasmuth 77.
Heller, V., 2011. Scale effects in physical hydraulic engineering models. J. ofHydraulic Res. 49, 293–306. https://doi.org/10.1080/00221686.2011.578914
Hewitt, K., 2002. Styles of rock avalanche depositional complexes conditioned by very rugged terrain, Karakoram Himalaya, Pakistan. Geol. Soc. Am. Rev. Eng. Geol. XV, 345–377.
Hewitt, K., 1998. Catastrophic landslides and their effects on the Upper Indus streams, Karakoram Himalaya, northern Pakistan. Geomorphology 26, 47–80. https://doi.org/10.1016/S0169-555X(98)00051-8
Hsü, K.J., 1975. Catastrophic debris streams (sturzstroms) generated by rockfalls. Bull. Geol. Soc. Am. https://doi.org/10.1130/0016-7606(1975)86<129:CDSSGB>2.0.CO;2
Hsu, L., Dietrich, W.E., Sklar, L.S., 2014. Mean and fluctuating basal forces generated by granular flows: Laboratory observations in a large vertically rotating drum. J. Geophys. Res. Earth Surf. 119, 1283–1309. https://doi.org/10.1002/2013JF003078
Hu, Y. xiang, Li, H. bo, Lu, G. da, Fan, G., Zhou, J. wen, 2021. Influence of size gradation on particle separation and the motion behaviors of debris avalanches. Landslides. https://doi.org/10.1007/s10346-020-01596-z
Hu, Y. xiang, Li, H. bo, Qi, S. chao, Fan, G., Zhou, J. wen, 2020. Granular Effects on Depositional Processes of Debris Avalanches. KSCE J. Civ. Eng. 24, 1116–1127. https://doi.org/10.1007/s12205-020-1555-3
Hughes, A., Kendrick, J.E., Salas, G., Wallace, P.A., Legros, F., Di Toro, G., Lavallée, Y., 2020. Shear localisation, strain partitioning and frictional melting in a debris avalanche generated by volcanic flank collapse. J. Struct. Geol. 140. https://doi.org/10.1016/j.jsg.2020.104132
Hungr, O., 2002. Rock Avalanche Occurrence, Process and Modelling, in: Evans, S., Scarascia-Mugnozza, G., Strom, A., Hermanns, R. (Eds.), Landslides from Massive Rock Slope Failure. Springer, Dordrecht, pp. 285–304.
Hungr, O., Evans, S., 2004. Entrainment of debris in rock avalanches: An analysis of a long run-out mechanism. Bull. Geol. Soc. Am. 116, 1240–1252. https://doi.org/10.1130/B25362.1
Hungr, O., Leroueil, S., Picarelli, L., 2014. The Varnes classification of landslide types, an update. Landslides 11, 167–194. https://doi.org/10.1007/s10346-013-0436-y
Iverson, R., 2015. Scaling and design of landslide and debris-flow experiments. Geomorphology 244, 9–20. https://doi.org/10.1016/j.geomorph.2015.02.033
Iverson, R., 1997. The physics of debris flows. Rev. Geophys. 35, 245–296. https://doi.org/10.1029/97RG00426
Iverson, R., Denlinger, R.P., 2001. Flow of variably fluidized granular masses across three-dimensional terrain: 1. Coulomb mixture theory. J. Geophys. Res. Solid Earth. https://doi.org/10.1029/2000JB900329
Iverson, R., Hooyer, T.S., Hooke, R.L., 1996. A laboratory study of sediment deformation: Stress heterogeneity and grain-size evolution. Ann. Glaciol. 22, 167–175. https://doi.org/10.1017/s0260305500015378
Iverson, R., Logan, M., Denlinger, R.P., 2004. Granular avalanches across irregular three-dimensional terrain: 2. Experimental tests. J. Geophys. Res. Earth Surf. 109, 1–16. https://doi.org/10.1029/2003jf000084
Iverson, R.M., Vallance, J.W., 2001. New views of granular mass flows. Geology 29, 115–118. https://doi.org/10.1130/0091-7613(2001)029<0115:NVOGMF>2.0.CO;2

Jiang, Y.J., Zhao, Y., 2015. Experimental investigation of dry granular flow impact via both normal and tangential force measurements. Geotech. Lett. 5, 33–38. https://doi.org/10.1680/geolett.15.00003

Knapp, S., Krautblatter, M., 2020. Conceptual Framework of Energy Dissipation During Disintegration in Rock Avalanches. Front. Earth Sci. 8, 1–9. https://doi.org/10.3389/feart.2020.00263

Kokelaar, B.P., Graham, R.L., Gray, J.M.N.T., Vallance, J.W., 2014. Fine-grained linings of leveed channels facilitate runout of granular flows. Earth Planet. Sci. Lett. 385, 172–180. https://doi.org/10.1016/j.epsl.2013.10.043

Lai, Z., Vallejo, L.E., Zhou, W., Ma, G., Espitia, J.M., Caicedo, B., Chang, X., 2017. Collapse of Granular Columns With Fractal Particle Size Distribution: Implications for Understanding the Role of Small Particles in Granular Flows. Geophys. Res. Lett. 44, 12,181-12,189. https://doi.org/10.1002/2017GL075689

Legros, F., 2002. The mobility of long-runout landslides. Eng. Geol. 63, 301–331. https://doi.org/10.1016/S0013-7952(01)00090-4

Li, K., Wang, Y.F., Lin, Q.W., Cheng, Q.G., Wu, Y., 2021. Experiments on granular flow behavior and deposit characteristics: implications for rock avalanche kinematics. Landslides 18, 1779–1799. https://doi.org/10.1007/s10346-020-01607-z

Linares-Guerrero, E., Goujon, C., Zenit, R., 2007. Increased mobility of bidisperse granular avalanches. J. Fluid Mech. 593, 475–504. https://doi.org/10.1017/S0022112007008932

Longchamp, C., Abellan, A., Jaboyedoff, M., Manzella, I., 2016. 3-D models and structural analysis of rock avalanches: The study of the deformation process to better understand the propagation mechanism. Earth Surf. Dyn. 4, 743–755. https://doi.org/10.5194/esurf-4-743-2016

Makris, S., Manzella, I., Cole, P., Roverato, M., 2020. Grain size distribution and sedimentology in volcanic mass-wasting flows: implications for propagation and mobility. Int. J. Earth Sci. https://doi.org/10.1007/s00531-020-01907-8

Makris, S., Roverato, M., Dávila-harris, P., Cole, P., Manzella, I., 2023a. Distributed stress fluidisation: Insights into the propagation mechanisms of the Abona volcanic debris avalanche (Tenerife) through a novel method for indurated deposit sedimentological analysis. Front. Earth Sci. 11, 1–22. https://doi.org/10.3389/feart.2023.1177507

Makris, S., Roverato, M., Lomoschitz, A., Cole, P., Manzella, I., Canaria, G., 2023b. The propagation and emplacement mechanisms of the Tenteniguada volcanic debris avalanche (Gran Canaria):Field evidence for brittle fault-accommodated spreading. J. Volcanol. Geotherm. Res. 435, 107773. https://doi.org/10.1016/j.jvolgeores.2023.107773

Mangeney, A., Roche, O., Hungr, O., Mangold, N., Faccanoni, G., Lucas, A., 2010. Erosion and mobility in granular collapse over sloping beds. J. Geophys. Res. Earth Surf. 115 (F3), 1–21. https://doi.org/10.1029/2009JF001462

Manzella, I., Einstein, H.H., Grasselli, G., 2013. DEM and FEM/DEM modelling of granular flows to investigate large debris avalanche propagation, in: Landslide Science and Practice: Spatial Analysis and Modelling. pp. 247–253. https://doi.org/10.1007/978-3-642-31310-3-33

Manzella, I., Labiouse, V., 2013. Empirical and analytical analyses of laboratory granular flows to investigate rock avalanche propagation. Landslides 10, 23–36. https://doi.org/10.1007/s10346-011-0313-5

Manzella, I., Labiouse, V., 2009. Flow experiments with gravel and blocks at small scale to

1147 investigate parameters and mechanisms involved in rock avalanches. Eng. Geol. 109, 146–
1148 158. https://doi.org/10.1016/j.enggeo.2008.11.006
1149 Manzella, I., Labiouse, V., 2008. Qualitative analysis of rock avalanches propagation by means
1150 of physical modelling of non-constrained gravel flows. Rock Mech. Rock Eng. 41, 133–
1151 151. https://doi.org/10.1007/s00603-007-0134-y
1152 McSaveney, M.J., 1978. Sherman glacier rock avalanche, alaska, U.S.A., Developments in
1153 Geotechnical Engineering. Elsevier Scientific Publishing Company.
1154 https://doi.org/10.1016/B978-0-444-41507-3.50014-3
1155 McSaveney, M.J., Davies, T., 2002. Rapid rock-mass flow with dynamic fragmentation:
1156 inferences from the morphology and internal structure of rockslides and rock avalanches, in:
1157 Evans, S., Scarascia Mugnozza, G., Strom, A., Hermanns, R. (Eds.), Landslides from
1158 Massive Rock Slope Failure. Springer, Dordrecht, pp. 285–304.
1159 McSaveney, M.J., Davies, T., Hodgson, K.A., 2000. A contrast in deposit style and process
1160 between large and small rock avalanches, in: Proceedings of the 8th International
1161 Symposium on Landslides, Cardiff, UK. pp. 26–30.
1162 Middleton, G. V, 1976. Subaqueous sediment transport and deposition by sediment gravity
1163 flows. Mar. sediment Transp. Environ. Manag. 197–218.
1164 Moro, F., Faug, T., Bellot, H., Ousset, F., 2010. Large mobility of dry snow avalanches: Insights
1165 from small-scale laboratory tests on granular avalanches of bidisperse materials. Cold Reg.
1166 Sci. Technol. 62, 55–66. https://doi.org/10.1016/j.coldregions.2010.02.011
1167 Okura, Y., Kitahara, H., Sammori, T., Kawanami, A., 2000. Effects of rockfall volume on runout
1168 distance. Eng. Geol. 58, 109–124. https://doi.org/10.1016/S0013-7952(00)00049-1
1169 Paguican, E.M., Roverato, M., Yoshida, H., 2021. Volcanic Debris Avalanche Transport and
1170 Emplacement Mechanisms, in: Roverato, M., Dufresne, A., Procter, J. (Eds.), Volcanic
1171 Debris Avalanches: From Collapse to Hazard. Springer book series advances in
1172 volcanology, pp. 143–173. https://doi.org/10.1007/978-3-030-57411-6_7
1173 Perinotto, H., Schneider, J.L., Bachèlery, P., Le Bourdonnec, F.X., Famin, V., Michon, L., 2015.
1174 The extreme mobility of debris avalanches: A new model of transport mechanism. J.
1175 Geophys. Res. Solid Earth. https://doi.org/10.1002/2015JB011994
1176 Phillips, J.C., Hogg, A.J., Kerswell, R.R., Thomas, N.H., 2006. Enhanced mobility of granular
1177 mixtures of fine and coarse particles. Earth Planet. Sci. Lett. 246, 466–480.
1178 https://doi.org/10.1016/j.epsl.2006.04.007
1179 Pierson, T.C., Costa, J.E., 1987. A rheologic classification of subaerial sediment-water flows.
1180 GSA Rev. Eng. Geol. 7, 1–12. https://doi.org/10.1130/REG7-p1
1181 Pollet, N., Schneider, J.L.M., 2004. Dynamic disintegration processes accompanying transport of
1182 the Holocene Flims sturzstrom (Swiss Alps). Earth Planet. Sci. Lett. 221, 433–448.
1183 https://doi.org/10.1016/S0012-821X(04)00071-8
1184 Pudasaini, S.P., Hutter, K., 2007. Avalanche dynamics: dynamics of rapid flows of dense
1185 granular avalanches. Springer Science & Business Media.
1186 Pudasaini, S.P., Wang, Y., Hutter, K., 2005. Rapid motions of free-surface avalanches down
1187 curved and twisted channels and their numerical simulation. Philos. Trans. R. Soc. A Math.
1188 Phys. Eng. Sci. 363, 1551–1571. https://doi.org/10.1098/rsta.2005.1595
1189 Rait, K.L., Bowman, E.T., 2016. Influences of strain rate and shear rate on the propagation of
1190 large scale rock avalanches. Landslides Eng. Slopes. Exp. Theory Pract. 3, 1707–1714.
1191 https://doi.org/10.1201/b21520-212
1192 Reubi, O., Hernandez, J., 2000. Volcanic debris avalanche deposits of the upper Maronne valley

(Cantal Volcano, France): Evidence for contrasted formation and transport mechanisms. J. Volcanol. Geotherm. Res. 102, 271–286. https://doi.org/10.1016/S0377-0273(00)00191-8

Reubi, O., Ross, P.S., White, J.D.L., 2005. Debris avalanche deposits associated with large igneous province volcanism: An example from the Mawson Formation, central Allan Hills, Antarctica. Bull. Geol. Soc. Am. 117, 1615–1628. https://doi.org/10.1130/B25766.1

Roche, O., Gilbertson, M.A., Phillips, J.C., Sparks, R.S.J., 2006. The influence of particle size on the flow of initially fluidised powders. Powder Technol. 166, 167–174. https://doi.org/10.1016/j.powtec.2006.05.010

Roche, O., van den Wildenberg, S., Valance, A., Delannay, R., Mangeney, A., Corna, L., Latchimy, T., 2021. Experimental assessment of the effective friction at the base of granular chute flows on a smooth incline. Phys. Rev. E 103, 042905. https://doi.org/10.1103/PhysRevE.103.042905

Roverato, M., Cronin, S., Procter, J., Capra, L., 2015. Textural features as indicators of debris avalanche transport and emplacement, Taranaki volcano. Bull. Geol. Soc. Am. 127, 3–18. https://doi.org/10.1130/B30946.1

Roverato, M., Dufresne, A., Procter, J., 2021. Volcanic Debris Avalanches: From collapse to Hazard.

Sanvitale, N., Bowman, E.T., 2016. Using PIV to measure granular temperature in saturated unsteady polydisperse granular flows. Granul. Matter 18, 1–12. https://doi.org/10.1007/s10035-016-0620-6

Savage, S.B., 1984. The mechanics of rapid granular flows. Adv. Appl. Mech. 24, 289–366.

Savage, S.B., Hutter, K., 1989. The motion of a finite mass of granular material down a rough incline. J. Fluid Mech. 199, 177–215.

Savage, S.B., Lun, C.K.K., 1988. Particle size segregation in inclined chute flow of dry cohesionless granular solids. J. Fluid Mech. 189, 311–335. https://doi.org/10.1017/S002211208800103X

Scheidegger, A.E., 1973. On the prediction of the reach and velocity of catastrophic landslides. Rock Mech. Felsmechanik Mécanique des Roches 5, 231–236. https://doi.org/10.1007/BF01301796

Schilirò, L., Esposito, C., De Blasio, F.V., Scarascia Mugnozza, G., 2019. Sediment texture in rock avalanche deposits: insights from field and experimental observations. Landslides 16, 1629–1643. https://doi.org/10.1007/s10346-019-01210-x

Schneider, J.L., Fisher, R. V., 1998. Transport and emplacement mechanisms of large volcanic debris avalanches: evidence from the northwest sector of Cantal Volcano (France). J. Volcanol. Geotherm. Res. 83, 141–165. https://doi.org/10.1016/S0377-0273(98)00016-X

Scott, K., Macias, J.L., Naranjo, J.A., Rodriguez, S., McGeehin, J.P., 2001. Catastrophic debris flows transformed from landslides in volcanic terrains: Mobility, hazard assessment, and mitigation strategies, US Geological Survey Professional Paper.

Scott, K., Vallance, J.W., Pringle, P.T., 1995. Sedimentology, behavior, and hazards of debris flows at Mount Rainier, Washington. U. S. Geol. Surv. Prof. Pap. 1547, 1–66. https://doi.org/10.1016/j.radonc.2016.01.020

Shea, T., van Wyk de Vries, B., 2008. Structural analysis and analogue modeling of the kinematics and dynamics of rockslide avalanches. Geosphere 4, 657–686. https://doi.org/10.1130/GES00131.1

Shreve, R.L., 1966. Sherman landslide, Alaska. Science (80-.). 154, 1639–1643.

Siebert, L., 2002. Landslides resulting from structural failure of volcanoes. GSA Rev. Eng. Geol.

15, 209–235. https://doi.org/10.1130/REG15-p209
Siebert, L., Glicken, H., Kienle, J., 1989. Debris avalanches and lateral blasts at Mount St Augustine volcano, Alaska. Natl. Geogr. Res. 5, 232–249.
Silbert, L.E., Ertaş, D., Grest, G.S., Halsey, T.C., Levine, D., Plimpton, S.J., 2001. Granular flow down an inclined plane: Bagnold scaling and rheology. Phys. Rev. E - Stat. Physics, Plasmas, Fluids, Relat. Interdiscip. Top. 64, 14. https://doi.org/10.1103/PhysRevE.64.051302
Thompson, N., Bennett, M.R., Petford, N., 2009. Analyses on granular mass movement mechanics and deformation with distinct element numerical modeling: Implications for large-scale rock and debris avalanches. Acta Geotech. 4, 233–247. https://doi.org/10.1007/s11440-009-0093-4
Ui, T., 1983. Volcanic dry avalanche deposits - Identification and comparison with nonvolcanic debris stream deposits. J. Volcanol. Geotherm. Res. 18, 135–150. https://doi.org/10.1016/0377-0273(83)90006-9
Ui, T., Glicken, H., 1986. Internal structural variations in a debris-avalanche deposit from ancestral Mount Shasta, California, USA. Bull. Volcanol. 48, 189–194. https://doi.org/10.1007/BF01087673
Valentino, R., Barla, G., Montrasio, L., 2008. Experimental analysis and micromechanical modelling of dry Granular flow and impacts in laboratory flume tests. Rock Mech. Rock Eng. 41, 153–177. https://doi.org/10.1007/s00603-006-0126-3
Vallance, J.W., 2000. Lahars. Encycl. volcanoes 601–616.
Vallance, J.W., Iverson, R., 2015. Lahars and Their Deposits, Second Edi. ed, The Encyclopedia of Volcanoes. Elsevier. https://doi.org/10.1016/b978-0-12-385938-9.00037-7
Van Gassen, W., Cruden, D.M., 1989. Momentum transfer and friction in the debris of rock avalanches. https://doi.org/10.1139/t89-075
van Wyk De Vries, B., Self, S., Francis, P.W., Keszthelyi, L., 2001. A gravitational spreading origin for the Socompa debris avalanche. J. Volcanol. Geotherm. Res. 105, 225–247. https://doi.org/10.1016/S0377-0273(00)00252-3
Voight, B., 1978. Rockslides and Avalanches. 1. Natural Phenomena. Elsevier, New York.
Voight, B., Janda, R.J., Glicken, H., Douglass, P.M., 1983. Nature and mechanics of the Mount St Helens rockslide-avalanche of 18 May 1980. Geotechnique 33, 243–273. https://doi.org/10.1680/geot.1983.33.3.243
Walton, O.R., 1993. Numerical simulation of inclined chute flows of monodisperse, inelastic, frictional spheres. Mech. Mater. 239–247.
Wang, Y.F., Cheng, Q.G., Shi, A.W., Yuan, Y.Q., Yin, B.M., Qiu, Y.H., 2019. Sedimentary deformation structures in the Nyixoi Chongco rock avalanche: implications on rock avalanche transport mechanisms. Landslides 16, 523–532. https://doi.org/10.1007/s10346-018-1117-7
Weidinger, J., Korup, O., Munack, H., Altenberger, U., Dunning, S., Tippelt, G., Lottermoser, W., 2014. Giant rockslides from the inside. Earth Planet. Sci. Lett. 389, 62–73. https://doi.org/10.1016/j.epsl.2013.12.017
Yang, Q., Cai, F., Ugai, K., Yamada, M., Su, Z., Ahmed, A., Huang, R., Xu, Q., 2011. Some factors affecting mass-front velocity of rapid dry granular flows in a large flume. Eng. Geol. 122, 249–260. https://doi.org/10.1016/j.enggeo.2011.06.006
Yang, Q., Su, Z., Cai, F., Ugai, K., 2015. Enhanced mobility of polydisperse granular flows in a small flume. Geoenvironmental Disasters 2, 12. https://doi.org/10.1186/s40677-015-0019-4

1285